Science of the Total Environment 999 (2025) 180327

Contents lists available at ScienceDirect

Science of the Total Environment

journal homepage: www.elsevier.com/locate/scitotenv

Ecological and carcinogenic risk assessment of potentially toxic elements in rangelands and croplands around Lake Junin (Peru): Integrating remote sensing, machine learning, and land cover segmentation

Samuel Pizarro [a,c,*], Edilson Requena-Rojas [a], Elgar Barboza [c], Eunice Peña-Elme [b], Alberto Arias-Arredondo [a], Dennis Ccopi [a]

[a] Estación Experimental Agraria Santa Ana, Dirección De Servicios Estratégicos Agrarios, Instituto Nacional de Innovación Agraria (INIA), Carretera Saños Grande – Hualahoyo Km 8 Santa Ana, Huancayo, Junín 12006, Peru
[b] Estación Experimental Agraria Santa Ana, Dirección de Desarrollo Tecnológico Agrario, Instituto Nacional de Innovación Agraria (INIA), Carretera Saños Grande-Hualahoyo Km 8 Santa Ana, Huancayo, Junín 12006, Peru
[c] Grupo de Investigación en Tecnologías Geoespaciales para la Agricultura de Precisión (GEOAP), Instituto de Investigación para el Desarrollo Sustentable de Ceja de Selva (INDES-CES), Universidad Nacional Toribio Rodríguez de Mendoza de Amazonas, Chachapoyas 01001, Peru

HIGHLIGHTS

- Random Forest mapped 14 PTEs across 211 highland samples with high precision.
- Arsenic, lead, and cadmium exceeded safety thresholds by over 100-fold.
- 99 % of study area showed very high to ultra-high ecological risk levels.
- 100 % carcinogenic risk for adults; children highly exposed to arsenic
- Vegetation cover types significantly influenced metal accumulation patterns.
- Multispectral indices enhanced contamination hotspot prediction accuracy.
- ML-remote sensing integration proved effective for highland risk assessment.

GRAPHICAL ABSTRACT

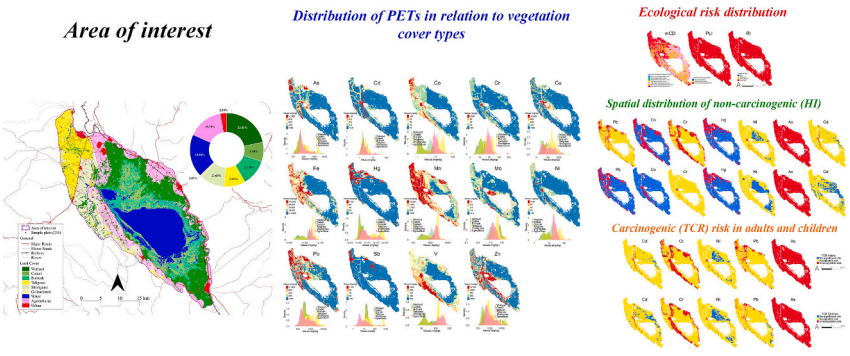

ARTICLE INFO

Keywords:
Heavy metals
Ecological risk assessment
Human health risk
Remote sensing
Machine learning
Soil contamination
Andean wetlands

ABSTRACT

The Junín Lake basin, a critical high-altitude ecosystem in the central Peruvian Andes, faces severe contamination from potentially toxic elements (PTEs) driven by mining activities, agriculture, and urbanization. This study evaluates the spatial distribution, ecological risk, and human health implications of 14 heavy metals, metalloids, and trace elements in surface soils surrounding the lake. Using 211 soil samples, we integrated remote sensing, land cover classification, and Random Forest machine learning models with spectral, edaphic, topographic, and proximity-based environmental covariates to predict contamination patterns and assess risk. Results reveal extreme contamination, with arsenic (As), lead (Pb), cadmium (Cd), and zinc (Zn) concentrations exceeding ecological thresholds by over 100-fold in agricultural zones. Ecological risk assessments using contamination degree (mCD), pollution load index (PLI), and risk index (RI) indicated that over 99 % of the study area exhibits very high to ultra-high contamination levels. Human health risk analysis identified unacceptable

* Corresponding author at: Estación Experimental Agraria Santa Ana, Dirección De Servicios Estratégicos Agrarios, Instituto Nacional de Innovación Agraria (INIA), Carretera Saños Grande – Hualahoyo Km 8 Santa Ana, Huancayo, Junín 12006, Peru.

https://doi.org/10.1016/j.scitotenv.2025.180327
Received 28 May 2025; Received in revised form 30 July 2025; Accepted 20 August 2025
Available online 27 August 2025

carcinogenic risks from As, Pb, and Cr across adult and pediatric populations, with arsenic presenting the greatest concern. The integration of geospatial tools and machine learning enabled precise identification of contamination hotspots and vulnerable land cover types, demonstrating the value of AI approaches for monitoring contaminated territories. These findings underscore the urgent need for coordinated environmental management, targeted remediation strategies, and community-based monitoring to protect public health and preserve Andean ecosystem integrity.

1. Introduction

Soil plays a fundamental role in ecosystem stability and global food security (Tiabou et al., 2024). However, increasing levels of contamination by various inorganic elements have generated growing environmental and health concerns. Among these contaminants, a group classified as potentially toxic elements (PTEs) stands out, which includes certain heavy metals, metalloids, and trace elements, characterized by their toxicity, persistence, and capacity for bioaccumulation in terrestrial and aquatic ecosystems (Hu et al., 2024). These elements can have a natural origin, such as weathering or geogenic processes, or come from anthropogenic activities, with mining being one of the most relevant sources, especially in high mountain regions under strong extractive pressure (Fu et al., 2025; Kong et al., 2025; Ullah et al., 2025).

The classification of PTEs according to their chemical nature and environmental behavior is fundamental to understanding the risks they represent. These are commonly grouped into heavy metals (such as Cd, Co, Cr, Cu, Hg, Ni, Pb, and Zn), metalloids (such as As and Sb), and trace elements (such as Fe, Mn, Mo, and V) (Hui et al., 2025; Lima et al., 2025; Tanwar et al., 2025). Each group presents distinct differences in terms of mobility, persistence, toxicity, and origin. While heavy metals and metalloids are often strongly linked to anthropogenic activities such as mining and are characterized by their high toxicity, trace elements, although essential in small quantities, become harmful when their concentrations exceed certain thresholds. Recognizing these distinctions is crucial for properly guiding environmental and health risk assessments, as well as developing effective monitoring and management strategies.

Elements such as As, Cd, Pb, Cu, and Zn have been extensively documented as hazardous when exceeding permissible limits, as they can cause damage to vital organs, neurological alterations, and increase the risk of chronic diseases, including various types of cancer (Mohammadi et al., 2023; Safadoust et al., 2025; Zhang et al., 2025). Beyond compromising ecological integrity, these contaminants affect agricultural and livestock productivity by interfering with plant metabolism, reducing crop yield and quality, and accumulating in the food chain (Vasilachi et al., 2023). This situation represents a direct threat to rural communities whose economies largely depend on agricultural and pastoral activities (Guo et al., 2020; Spater et al., 2024).

Understanding the spatial distribution of PTEs in soil is essential for mitigating their impacts. However, this is complicated by high soil heterogeneity and the irregular distribution of contamination sources (Guo et al., 2020; Vasudhevan et al., 2025). In response to these challenges, innovative approaches based on digital soil mapping, geostatistics, and machine learning (ML) have been developed, which have significantly improved the accuracy of contaminant concentration predictions (Yang and Jia, 2024).

Among ML algorithms, the Random Forest (RF) model has proven particularly effective for this type of analysis. Its predictive capacity is substantially enhanced when combined with multispectral remote sensing data, geochemical analyses, and environmental variables. Spectral indices such as the Normalized Difference Water Index (NDWI), Normalized Burn Ratio (NBR), and Soil-Adjusted Vegetation Index (SAVI) (Guo et al., 2024; Tan et al., 2020), along with topographic variables, land use classifications, and soil physicochemical properties, provide highly relevant predictive information. This multidisciplinary integration enables more robust and reliable estimates, which are further strengthened by sophisticated land cover segmentation techniques that distinguish areas with different levels of exposure and response to contamination (Ma et al., 2025; Salgado et al., 2023; Sun et al., 2024).

The ecological environment, serving as an essential foundation for life and human development, is increasingly threatened by the accumulation of potentially toxic elements, whose presence can severely disrupt ecosystem functionality (Li et al., 2025a). To assess the ecological risk posed by these contaminants, standardized indices such as the ecological risk index (Er) and the potential ecological risk index (PERI) are commonly employed, complemented by diagnostic parameters including the contamination factor (CF), enrichment factor (EF), geoaccumulation index (Igeo), and pollution load index (PLI). These indicators enable comprehensive estimation of both the intensity and spatial extent of environmental degradation caused by PTEs, providing a quantitative foundation for evidence-based environmental management and risk mitigation strategies (Duman et al., 2025; Hakanson, 1980; Siddig et al., 2025a).

Regarding carcinogenic and non-carcinogenic health risks, human exposure to PTEs through multiple pathways including ingestion, inhalation, and dermal contact represents a critical public health concern, particularly in relation to elements such as Pb, As, and Cd (Ahmad et al., 2025; Khoshakhlagh et al., 2024). For comprehensive health risk evaluation, standardized metrics such as the non-carcinogenic risk index (HI) and carcinogenic risk (CR) are applied, following the guidelines established by the United States Environmental Protection Agency (US-EPA) (Shen et al., 2021).

Peru experiences the environmental challenges common to mining-intensive developing countries, where extractive industries offer significant economic benefits but also pose substantial ecological risks. As the world's second-largest producer of copper, silver, and zinc, Peru has experienced widespread environmental degradation in its high Andean regions, particularly in areas composed of rangelands and croplands (Caicedo-Rivas et al., 2023; Cruzado-Tafur et al., 2021).

One of the most striking examples of mining-related impacts is observed in the San Juan River basin. The construction of the Upamayo Dam in 1932 fundamentally altered the regional hydrology by diverting contaminated waters from the San Juan River, which originally flowed into the Mantaro River, directly into Lake Junín. This anthropogenic intervention has been especially harmful during the dry season, when lake levels typically decrease by approximately 2 m, leading to the concentration of contaminant loads (Rodbell et al., 2014).

The San Juan River is the primary inflow to Lake Junín, with an average annual flow of 286.03 million m^3 and recorded extremes ranging from 114.7 to 1.01 $m^{3/s}$. It transports elevated concentrations of heavy metals resulting from intensive mining activities, including discharges from the AUREX gold mine, abandoned tailings deposits, and untreated wastewater (Custodio et al., 2019). As a result, Lake Junín has become a depository of mining-derived pollutants. This situation has seriously affected aquatic biodiversity and degraded water quality to the point where it is unsuitable for irrigation and other productive uses (Guo et al., 2020; Hoang et al., 2025; Moreno-Aguirre et al., 2024).

For decades, Lake Junín has been exposed to pollution from multiple sources, generating growing concern over its ecological integrity and the safety of its water resources (del Sante et al., 2025). Given the lake's critical role in supporting surrounding rangeland and cropland systems, a comprehensive assessment of contamination is urgently needed from

both environmental and public health perspectives.

Addressing this critical environmental challenge, the present study aims to conduct a comprehensive assessment of the ecological and carcinogenic risks associated with the presence of PTEs in rangelands and croplands surrounding the Junin Lake. This research integrates cutting-edge methodological approaches, including remote sensing technologies, advanced ML algorithms (specifically RF), and sophisticated land cover segmentation techniques, to achieve multiple objectives: identify areas of greatest environmental vulnerability, accurately estimate the spatial distribution of soil contaminants across different land use types, and quantify their potential impacts on both human health and ecosystem integrity. This integrated methodological framework represents a significant advancement in environmental risk assessment for high-altitude mining-impacted regions, providing a robust technical foundation for evidence-based environmental management, policy development, and informed decision-making. The results will contribute to the broader understanding of PTE contamination patterns in Andean highland agricultural systems and support the development of targeted remediation and risk mitigation strategies for similar environments globally.

2. Materials and methods

2.1. Study area

Junín Lake (Chinchaycocha), situated in the central Peruvian Andes at 4100 m above sea level (11°01′12″S, 76°06′27″W), represents Peru's second-largest lacustrine system with a surface area of 529 km^2 and maximum depth of 12 m (Cusiche and Miranda, 2019; Cusiche Pérez, 2017). As the headwater source of the Mantaro River, a principal tributary within the Amazon basin, this high-altitude lake system plays a crucial hydrological role in regional water resources. The lake is encompassed within Junín National Park and embedded within characteristic puna ecosystems, including extensive high-altitude grasslands, wetland complexes, and peat bog formations that are endemic to Andean highland environments (Fig. 1).

Despite its ecological significance and protected status, Junín Lake faces severe anthropogenic pressures that threaten its ecosystem integrity. Mining activities within the watershed have emerged as the primary degradation driver, introducing heavy metal contamination that compromises water quality, soil chemistry, and the stability of associated terrestrial and aquatic ecosystems (Martin et al., 2001). This environmental degradation represents a critical conservation challenge for one of Peru's most important high-altitude aquatic ecosystems, necessitating urgent assessment and management intervention to preserve its ecological functions and biodiversity.

2.2. Sampling design, collection and analytical procedures

Sampling points were established using a systematic radial grid with 2-km intervals around Junín Lake, following the methodological framework outlined by FAO (2000) for contaminated soil assessment. A total of 211 soil samples were collected and uniformly distributed across the study area to ensure representative spatial coverage. Each sampling point consisted of a composite sample comprising five subsamples: one collected at the central coordinates and four additional subsamples collected at the vertices of a 5-m × 5-m square centered on the sampling point. This composite sampling design was implemented to capture

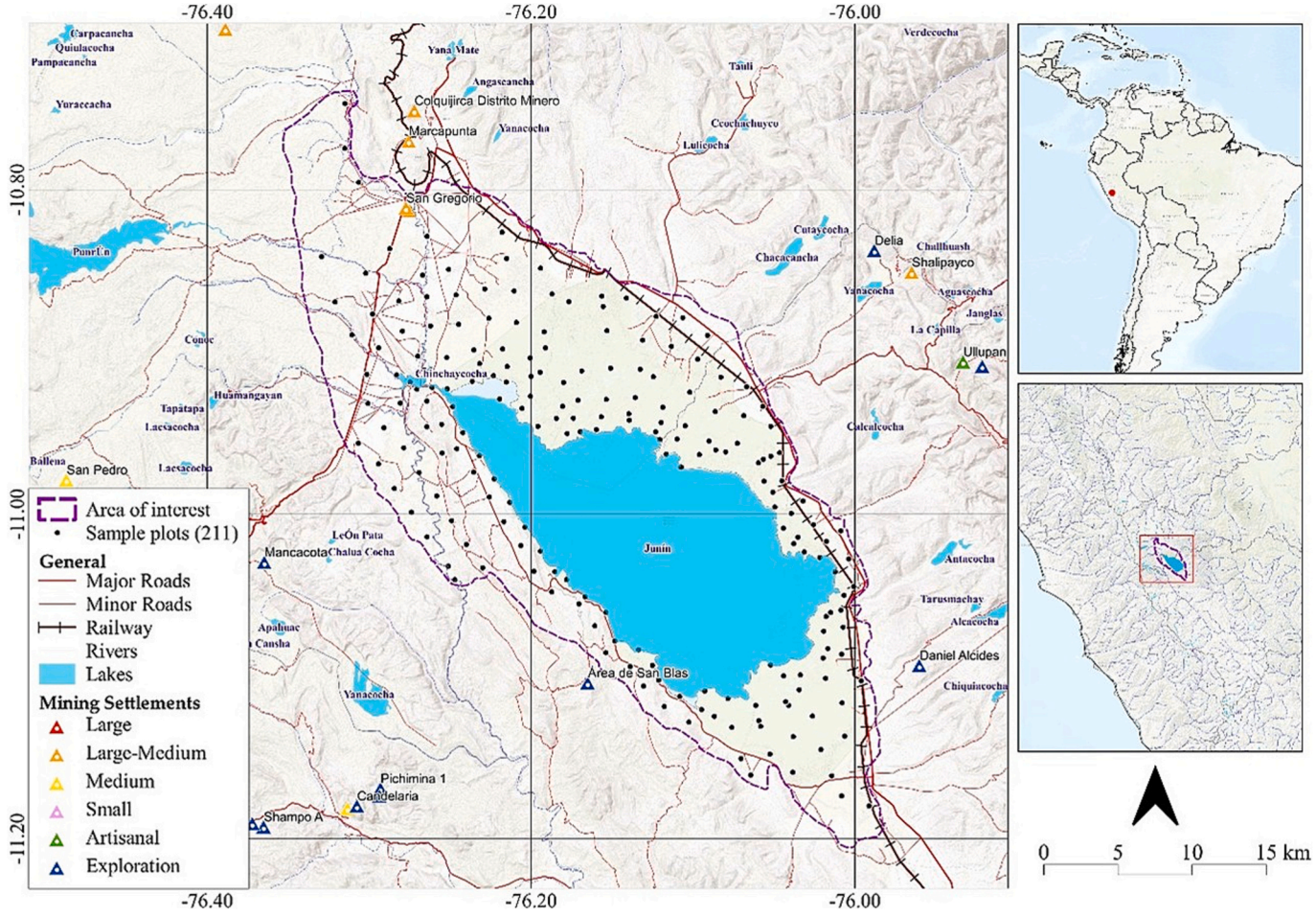

Fig. 1. Location map of soil sampling sites around Lake Junín.

small-scale spatial variability while maintaining statistical representativeness. All samples were collected from the 0–30 cm depth interval, representing the surface soil horizon where contaminant accumulation is typically highest and interactions with anthropogenic activities are most pronounced FAO (2000).

The determination of PTEs was conducted at the Soil, Water and Foliar Analysis Laboratory (LABSAF), Santa Ana, National Institute for Agricultural Innovation (INIA). Soil samples underwent acid digestion following EPA Method 3050B (EPA Method 3050B, 1996) and were subsequently analyzed using inductively coupled plasma optical emission spectrometry (ICP-OES) in accordance with EPA Method 6010D (EPA Method 6010D, 2018). This analytical approach enabled the quantification of 14 PTEs: arsenic (As), cadmium (Cd), cobalt (Co), chromium (Cr), copper (Cu), iron (Fe), manganese (Mn), mercury (Hg), molybdenum (Mo), nickel (Ni), lead (Pb), antimony (Sb), vanadium (V), and zinc (Zn). Quality assurance and quality control procedures included the analysis of certified reference materials, method blanks, and duplicate samples to ensure analytical precision and accuracy.

2.3. Covariate analysis

Six groups of environmental covariates were selected as predictors for the RF model to estimate spatial metal distribution (Table 1). These covariates encompass spectral variables derived from Sentinel-2 reflectance bands (blue, red, NIR) that capture surface reflectance variations indicative of soil and vegetation changes. Spectral indices include the Normalized Difference Vegetation Index (NDVI), Enhanced Vegetation Index (EVI), and Modified Soil-Adjusted Vegetation Index (MSAVI) quantify vegetation vigor, moisture content, and physiological stress conditions. Climatic and hydrological variables (precipitation, temperature, potential evapotranspiration, flood occurrence) influence soil moisture dynamics and facilitate contaminant transport processes.

Table 1
Environmental covariates used in RF modeling.

Group	Covariates	Description
Spectral	blue, green, red, red_edge_1, red_edge_2, red_edge_3, red_edge_4, nir, swir1, swir2	Sentinel-2 multispectral reflectance bands. Detect surface reflectance changes in soil and vegetation indicating physical or chemical alterations (Wang et al., 2024).
Spectral indices	NDVI, NBR, NDWI, MSAVI, EVI, SVVI, BRIGHT, GREEN, WET	Vegetation and soil condition indices derived from band combinations. Quantify vegetation vigor, moisture content, canopy structure, and stress conditions commonly used in soil quality assessments (Moura-Bueno et al., 2021).
Climatic & hydrological	precipitac, t_min, t_max, pte, Flood	Climate and hydrology variables controlling soil moisture dynamics and contaminant transport mechanisms (Moura-Bueno et al., 2021).
Topographic	Elevation, Slope, Aspect, Hillshade, Northness, Eastness, Horizontal, VerticalCu, MeanCurvat, GaussianCu	Terrain morphology parameters affecting runoff, erosion processes, and metal accumulation patterns (Agyeman et al., 2022).
Soil properties	clay, sand, silt, SOC, CEC, bdod, nitrogen, pH	Physicochemical soil characteristics controlling metal retention, mobility, and biogeochemical interactions (Kasraei et al., 2024).
Distance factors	D_rivers, D_Mroads, D_mroads, D_ferrc, D_lag	Euclidean distances to anthropogenic and natural features representing contamination pressure and dispersal pathways (Paes et al., 2022).

Topographic features such as elevation, slope, and curvature parameters control surface runoff patterns and metal accumulation zones. Soil physicochemical properties including clay content, soil organic carbon (SOC), and pH regulate metal retention capacity and mobility within the soil matrix. Distance factors representing proximity to rivers, roads, and lakes serve as proxies for potential contamination sources and dispersal pathways.

2.4. Machine learning model

Random Forest (RF), a supervised ensemble learning algorithm, was employed for predicting heavy metal concentrations due to its capacity to model complex nonlinear relationships and handle high-dimensional datasets. The RF algorithm constructs multiple decision trees using bootstrap aggregating (bagging) from random subsets of training data and predictor variables, subsequently combining their predictions through majority voting for classification or averaging for regression tasks. This approach enhances prediction accuracy while reducing overfitting and providing robust variable importance rankings (Kasraei et al., 2024).

The RF model utilized the comprehensive covariate dataset including spectral bands, soil physicochemical properties, topographic parameters, climatic variables, and proximity indices to predict spatial heavy metal distributions. Beyond generating high-precision contamination maps, the algorithm quantified the relative importance of each predictor variable using mean decrease in impurity metrics, facilitating interpretation of contamination drivers and informing targeted remediation strategies (Paes et al., 2022).

2.5. Vegetation cover classification

Vegetation cover maps were generated through supervised classification of multitemporal multispectral imagery using the Google Earth Engine (GEE) cloud computing platform (Gorelick et al., 2017). The analysis incorporated Sentinel-2 surface reflectance imagery collected from June to August over the past five years, with cloud-free imagery selected and temporally reduced using median compositing to minimize atmospheric interference and seasonal variations.

Training and validation data consisted of 9000 randomly selected pixel samples (1000 per vegetation class), with 80 % derived from field observations and 20 % from visual interpretation of high-resolution Google Earth imagery, supplemented by reference data from the 2015 National Vegetation Map (Ministerio del Ambiente, 2015) and the classification map developed by Cano et al. (2023). The dataset was partitioned into training (70 %) and validation (30 %) subsets using stratified random sampling to ensure statistical independence and representative class distribution.

Supervised RF classification was implemented incorporating both spectral characteristics of high Andean vegetation communities and topographic variables derived from the Advanced Land Observing Satellite Phased Array L-band Synthetic Aperture Radar (ALOS PALSAR) digital elevation model. Key topographic parameters included elevation, slope, and aspect, which significantly influence vegetation distribution patterns in mountainous terrain. The classification process generated vegetation maps at 10-m spatial resolution, following methodological approaches established by Pizarro et al. (2022).

2.6. Ecological and carcinogenic risk assessment

This study conducted an integrated assessment of ecological and carcinogenic risks associated with heavy metal contamination in agricultural and grazing soils surrounding Junín Lake. The ecological risk assessment evaluated contamination effects on ecosystem integrity and associated ecosystem services through exposure estimation and hazard characterization of environmental chemical substances (Gan et al., 2022; Yang et al., 2024).

2.6.1. Ecological risk assessment methodology

Average concentrations of the upper continental crust (Taylor and Mclennan, 1995) served as reference values, with iron (Fe) as the baseline element for enrichment factor (EF) calculations. Additional geochemical indices were computed to determine environmental alteration levels caused by PTEs: the contamination factor (CF) and geo-accumulation index (Igeo) (Hakanson, 1980; Li et al., 2025a). The pollution load index (PLI) was calculated to summarize overall multi-element contamination levels, while the mean contamination degree (mCD) quantified individual element contributions to total ecological risk (Reimann and De Caritat, 2005; Tomlinson et al., 1980; Victoria et al., 2014). These indicators were integrated to estimate the ecological risk index (RI), enabling classification of study areas by ecological risk level. Detailed calculation formulae are provided in Table S1.

2.6.2. Human health risk assessment

Human health risk estimation employed USEPA-recommended formulae to calculate chronic daily dose (CDD) through three exposure pathways: ingestion, inhalation, and dermal contact (Eqs. 1–3). Parameters included metal concentration (CM), ingestion rate (IR), inhalation rate (IHR), dermal contact area (SA), average body weight (ABW), exposure duration and frequency (ED, EF), among others (Cui et al., 2023). Non-carcinogenic risks were quantified using the hazard index (HI) (Eq. 4), while carcinogenic risks (CR) for each pathway were estimated using slope factors (SF) and inhalation unit risk (IUR) values. Total carcinogenic risk (TCR) was calculated as the sum of individual pathway risks from ingestion, inhalation, and dermal absorption (Eq. 5).

2.6.3. Spatial risk analysis

Results were integrated with remote sensing data, ML algorithms, and land cover segmentation techniques to generate comprehensive spatial risk maps. These maps facilitate identification of critical contamination zones and provide guidance for targeted environmental and health remediation strategies (Li et al., 2025c; Lovynska et al., 2024).

$$CDD_{ingestion} = \frac{CM \times IR \times ED \times EF}{ABW \times AET} \times Cf \tag{1}$$

$$CDD_{inhalacion} = \frac{CM \times IHR \times ED \times EF}{ABW \times AET \times PEF} \tag{2}$$

$$CDD_{dermal} = \frac{CM \times SA \times SAF \times DAF \times ED \times EF}{ABW \times AET} \times Cf \tag{3}$$

$$HI = \sum HQ_{ind/inh/der} \tag{4}$$

$$TCR = \sum CR_{ing/inh/der} \tag{5}$$

Eqs. (1)–(3) estimate the chronic daily dose (CDD, mg/kg·day) via ingestion, inhalation, and dermal contact, which are considered by the EPA (1996) and US-EPA (2004) as the main exposure pathways to soil contaminants. The parameters used include: CM (metal concentration in soil, mg/kg), IR (soil ingestion rate, mg/day), IHR (inhalation rate, m^3/day), SA (exposed skin area, cm^2), SAF (soil adherence factor, mg/cm^2), DAF (dermal absorption factor), ED (exposure duration, years), EF (exposure frequency, days/year), ABW (average body weight, kg), AET (average exposure time, days), Cf (conversion factor, 10^{-6} kg/mg), and PEF (particle emission factor, m^3/kg). These pathways are particularly relevant in agricultural and inhabited areas such as the surroundings of Lake Junín, where people are frequently in contact with soil. Unintentional soil ingestion is more common among children, while inhalation of dust and dermal contact mainly affect adults under chronic exposure conditions (Hongxing Zhang et al., 2019). The specific values used for each age group are detailed in Supplementary Table S7.

2.7. Statistical analysis

All statistical analyses and predictive modeling were conducted using R software (version 4.1.2; R Core Team, 2021). Prior to analysis, data preprocessing included outlier detection and removal, normality assessment, and variable selection using the tidyverse (Wickham et al., 2019) and caret packages (Kuhn, 2008).

Descriptive statistics (mean, standard deviation, variance, minimum, and maximum values) were computed using base R functions and the dplyr package (Wickham et al., 2019). Pearson product-moment correlation coefficients were calculated to assess linear relationships between variables, with correlation matrices visualized using the corrplot package (Wei and Simko, 2010). Principal component analysis (PCA) was performed using the FactoMineR package (Lê et al., 2008) to identify underlying data structure and reduce dimensionality.

For prediction of PTEs, RF regression models were implemented using the randomForest package (Liaw and Wiener, 2002). Model performance was evaluated using k-fold cross-validation (k = 10) with metrics including root mean square error (RMSE), mean absolute error (MAE), and coefficient of determination (R^2). Variable importance was assessed using the mean decrease in accuracy and Gini impurity measures.

Geospatial deployment and visualization of predictive models were conducted on the GEE platform (Gorelick et al., 2017), enabling large-scale spatial analysis and mapping of PTE distributions.

3. Results

3.1. Descriptive statistics of PTEs

The statistical analysis of PTEs revealed substantial variability in concentrations across the study area (Table 2), with highly skewed distributions indicating localized contamination hotspots. Several heavy metals exhibited severe contamination, significantly exceeding established sediment quality guidelines. Lead reached maximum concentrations of 15,767.65 mg/kg, exceeding the Probable Effect Level (PEL: 112.0 mg/kg) by 141-fold. Similarly, zinc (max: 30,576.88 mg/kg), copper (max: 7694.61 mg/kg), and mercury (max: 1661.89 mg/kg) substantially surpassed their respective PEL values by factors of >100, 71, and 2374, respectively.

Arsenic demonstrated considerable contamination potential with maximum concentrations of 4224.61 mg/kg, exceeding the PEL (41.6 mg/kg) by approximately 100-fold. Antimony concentrations varied widely (max: 769.27 mg/kg), though established guidelines are unavailable. Trace elements including iron (max: 228,937.50 mg/kg), manganese, molybdenum, and vanadium showed elevated concentrations reflecting both natural geological processes and anthropogenic influences.

The substantial exceedances of ecological benchmarks (TEL and PEL) for multiple elements indicate significant contamination that may pose ecological risks to benthic organisms and associated food webs (Ettler, 2016; Nawrot et al., 2021).

3.2. Vegetation cover classification

Fig. 2 presents the land cover classification for the lands around Junin Lake, derived through RF algorithm analysis. Nine distinct land cover classes were identified: wetlands, emergent vegetation (predominantly cattail and bulrush), high-density grasslands, low-density grasslands, gelifluction-affected areas, agricultural lands, urban areas, and the lake water body. The corresponding area distribution analysis reveals that wetlands and water bodies constitute the dominant land cover types within the study region. This classification framework provides the spatial foundation for subsequent analysis of land cover influences on the distribution patterns and environmental fate of PTEs throughout the watershed.

Table 2
Descriptive statistics of PTEs.

Category	Element	Mean	SD	Max	TEL (mg/kg)	PEL (mg/kg)
Heavy metals	Cd	3.09	9.94	97.27	0.676	4.21
	Cr	20.87	28.50	297.47	52.3	160.0
	Cu	234.47	816.25	7694.61	18.7	108.0
	Hg	13.92	120.04	1661.89	0.13	0.70
	Ni	17.79	29.31	313.77	15.9	42.8
	Pb	553.49	1753.12	15,767.65	30.2	112.0
	Zn	1360.51	4855.03	30,576.88	124.0	271.0
Metalloids	As	288.07	506.69	4224.61	7.24	41.6
	Sb	16.98	57.86	769.27	–	–
Trace elements	Fe	17,511.52	28,114.95	228,937.50	–	–
	Mn	1278.49	1636.13	12,258.18	–	–
	Mo	1.33	1.19	7.10	–	–
	V	84.58	64.13	329.12	–	–

Note: All concentrations are expressed in mg/kg dry weight. TEL = threshold effect level; PEL = probable effect level. Standard deviations (SD) indicate high variability in elemental distributions across sampling locations.

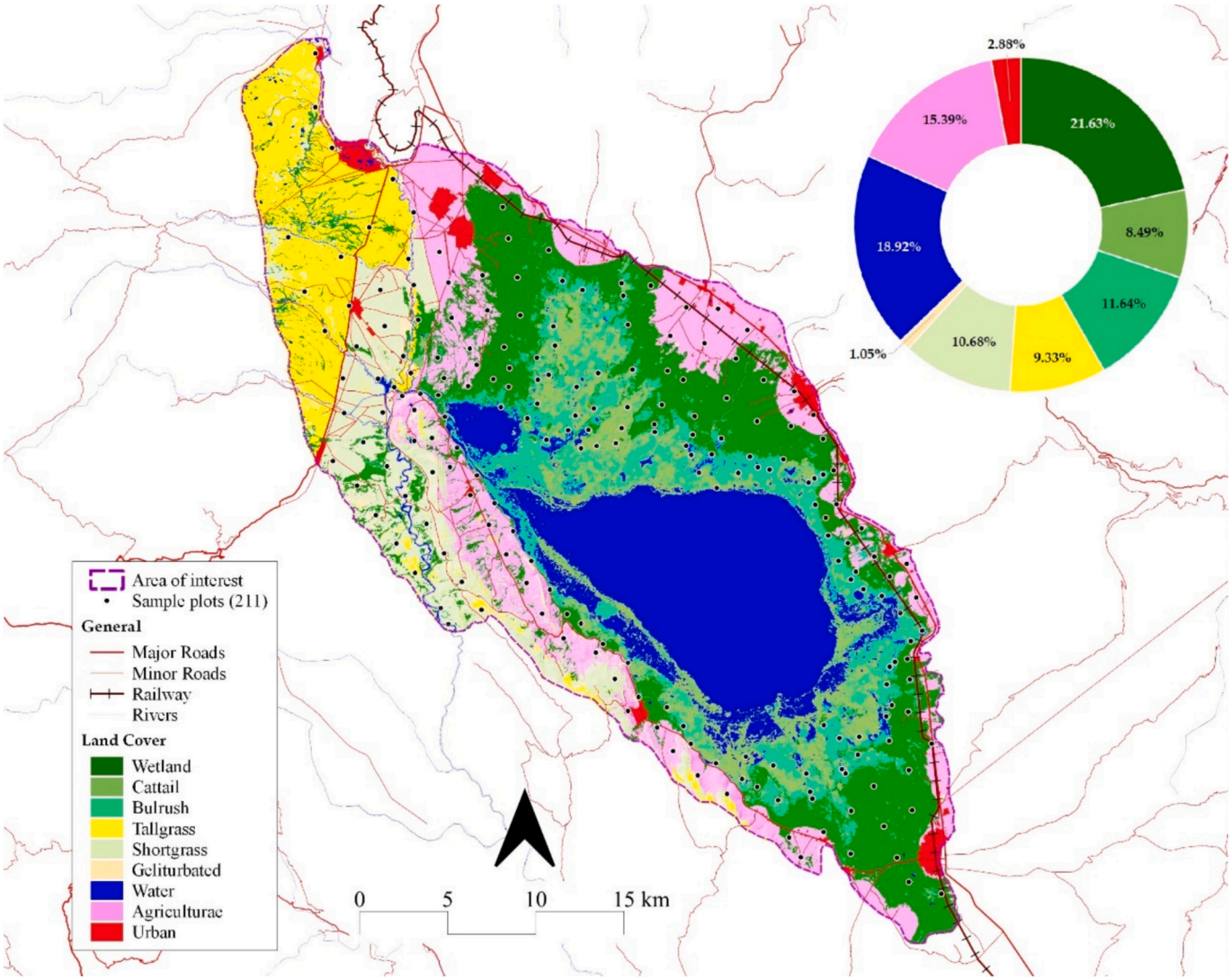

Fig. 2. Land cover classification of lands around Junin Lake derived from RF classification algorithm.

3.3. PCA of vegetation cover and PTEs

Fig. 3a illustrates the multivariate relationships between vegetation cover types surrounding Junin Lake and key environmental variables, including elevation, aspect, terrain shading, spectral indices, and soil physicochemical properties (pH, clay content, organic matter content, and cation exchange capacity). The ordination analysis reveals that bulrushes, wet grasslands, and wetland communities form distinct clusters, suggesting their association with environmentally stable conditions characterized by minimal anthropogenic disturbance.

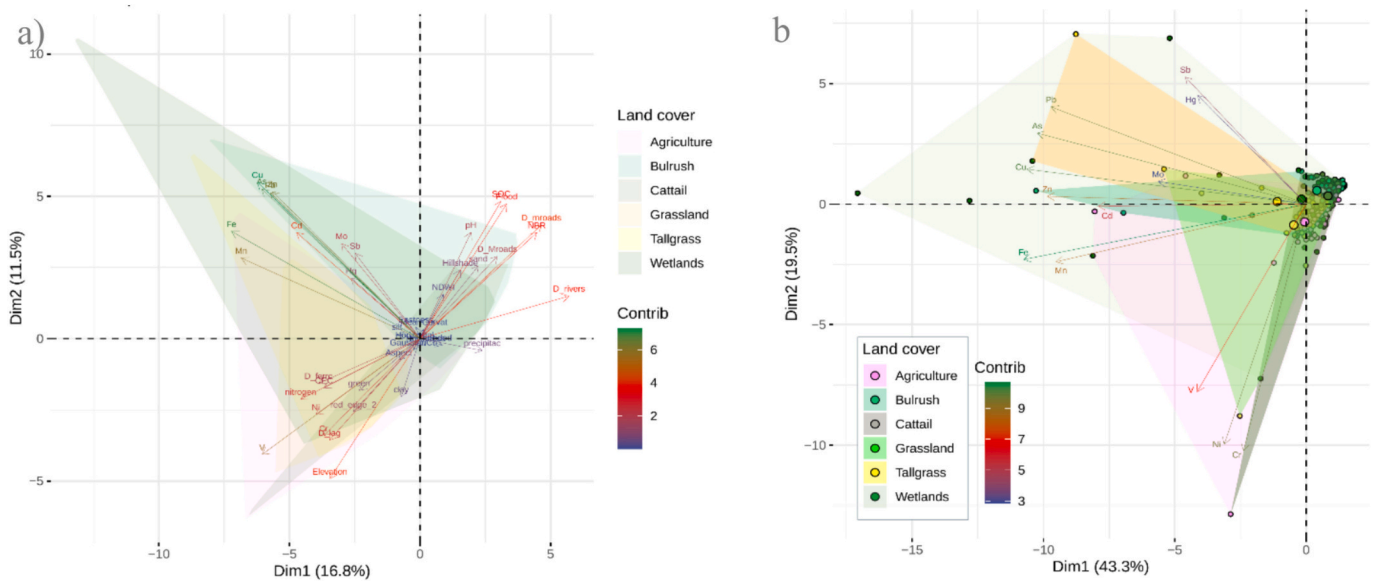

Fig. 3. Principal component analysis (PCA) applied to vegetation cover around Junin Lake. (a) Relationship between vegetation cover, environmental variables, and soil properties; (b) association between vegetation cover and PTEs.

Conversely, agricultural areas and tallgrass vegetation are associated with specific soil and topographic conditions that correspond to zones with elevated potential for accumulation of PTEs, including arsenic (As), cadmium (Cd), and lead (Pb). These land cover types may possess limited capacity for heavy metal attenuation.

Fig. 3b demonstrates strong positive associations between PTE concentrations and both agricultural areas and cattail (*Typha* spp.) vegetation, particularly for As, Cd, and Pb, indicating elevated contaminant accumulation in these zones. In contrast, bulrush communities and other wetland vegetation types exhibit weak or non-significant associations with the analyzed heavy metals, suggesting either lower contaminant loading or enhanced natural sequestration capacity. This spatial differentiation enables the identification of vegetation communities that serve as either sensitive indicators or accumulators of environmental contamination. These findings provide critical baseline information for developing targeted environmental monitoring protocols, remediation strategies, and adaptive management approaches within the Junin Lake watershed.

3.4. Correlation between variables

Fig. 4 presents a correlation matrix of pairwise Pearson correlation coefficients among predictor variables used to model PTEs spatial distribution in soils surrounding Junin Lake. The matrix includes spectral, topographic, edaphic, and anthropogenic proximity variables, using a diverging color scale (blue: positive, red: negative, white: null correlations) with statistically non-significant correlations ($p > 0.05$) marked by black "×".

The correlation structure reveals distinct clustering patterns. Spectral variables (green, red_edge_2, NDWI, NBR, precipitation) show moderate to strong positive correlations due to shared sensitivity to vegetation and moisture gradients. Topographic variables (Elevation, Aspect, Hillshade, Northness, Eastness) exhibit weak to moderate correlations, notably between Hillshade and Northness reflecting solar incidence patterns. Edaphic variables demonstrate strong intercorrelations, particularly SOC-CEC and clay-CEC relationships, consistent with soil texture-nutrient retention dependencies. Conversely, anthropogenic distance variables (D_rivers, D_Mroads, D_ferrc) show weak correlations with environmental variables, indicating independent spatial processes. This pattern confirms that selected variables provide balanced thematic relevance and data diversity, enhancing model predictive performance.

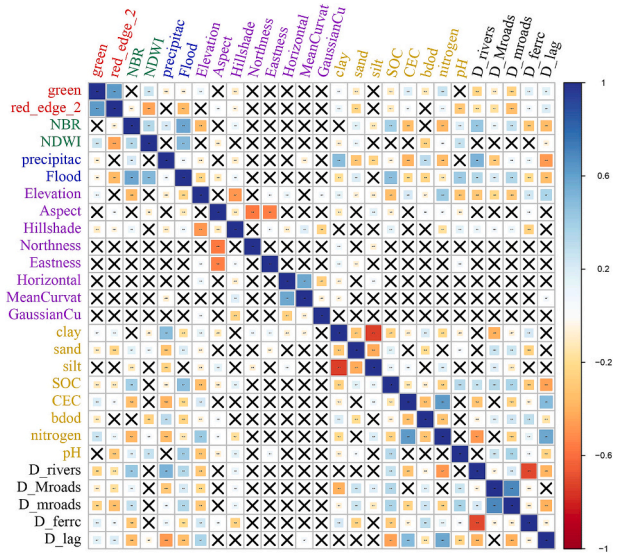

Fig. 4. Correlation matrix.

3.5. Model performance

Fig. 5 shows the performance of RF models used to estimate the concentrations of 14 heavy metals in soils, including As, Cd, Co, Cr, Cu, Fe, Hg, Mn, Mo, Ni, Pb, Sb, V, and Zn. The parallel coordinate plots illustrate the variation in model performance across different hyperparameter combinations, assessed through R^2, RMSE, MAE, and RPD metrics.

All elements demonstrated strong predictive performance with $R^2 \geq 0.95$ and RPD > 2.5. Copper, nickel, and zinc achieved exceptional accuracy ($R^2 > 0.97$; RPD > 4.0), while lead and chromium showed greater error variability but remained robust. Metalloids performed favorably: arsenic achieved high accuracy ($R^2 = 0.969$; RPD = 4.27) despite spatial variability, and antimony maintained acceptable performance ($R^2 = 0.939$; RPD = 2.97). Trace elements exhibited excellent

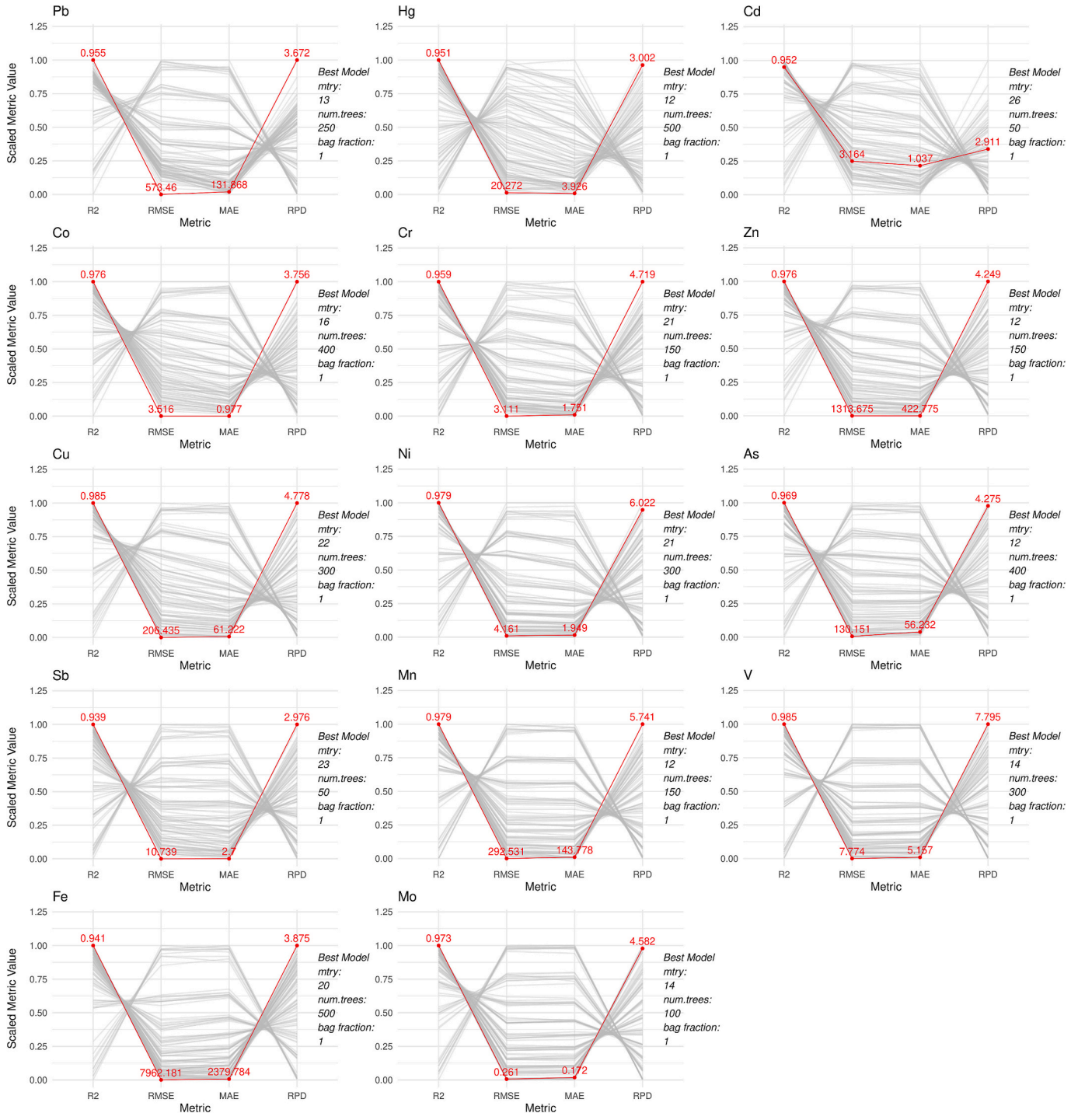

Fig. 5. Predictive performance of the RF model for heavy metals based on hyperparameter tuning and evaluation metrics (R^2, RMSE, MAE, and RPD).

characteristics: vanadium and manganese achieved outstanding accuracy (RPD > 5.0; $R^2 > 0.97$), molybdenum showed notable precision ($R^2 = 0.973$; MAE ≈ 0.17) despite low concentrations, and iron maintained satisfactory performance ($R^2 = 0.941$; RPD = 3.87) despite natural variability.

3.6. Distribution of PTEs in relation to vegetation cover types around Junin Lake

Fig. 6 shows spatial distribution maps and kernel density estimates of 14 heavy metals, transition elements, and trace elements in surface soils surrounding Junin Lake, stratified by vegetation cover types (wetland, cattail, bulrush, tallgrass, shortgrass, and agricultural lands).

Spatial patterns reveal distinct enrichment zones with hotspots concentrated in northern and eastern sectors, particularly for Hg, Pb, Zn, Cu, and Fe, reflecting anthropogenic influences from agriculture, runoff, or legacy contamination. Agricultural lands consistently exhibit the highest metal concentrations and broadest distributions, especially for Cd, Zn, Cu, and Pb, suggesting inputs from fertilizers and agrochemicals. In contrast, natural vegetation covers (wetlands, cattails, moist pastures) display significantly lower concentrations and narrower distributions, indicating important buffering functions.

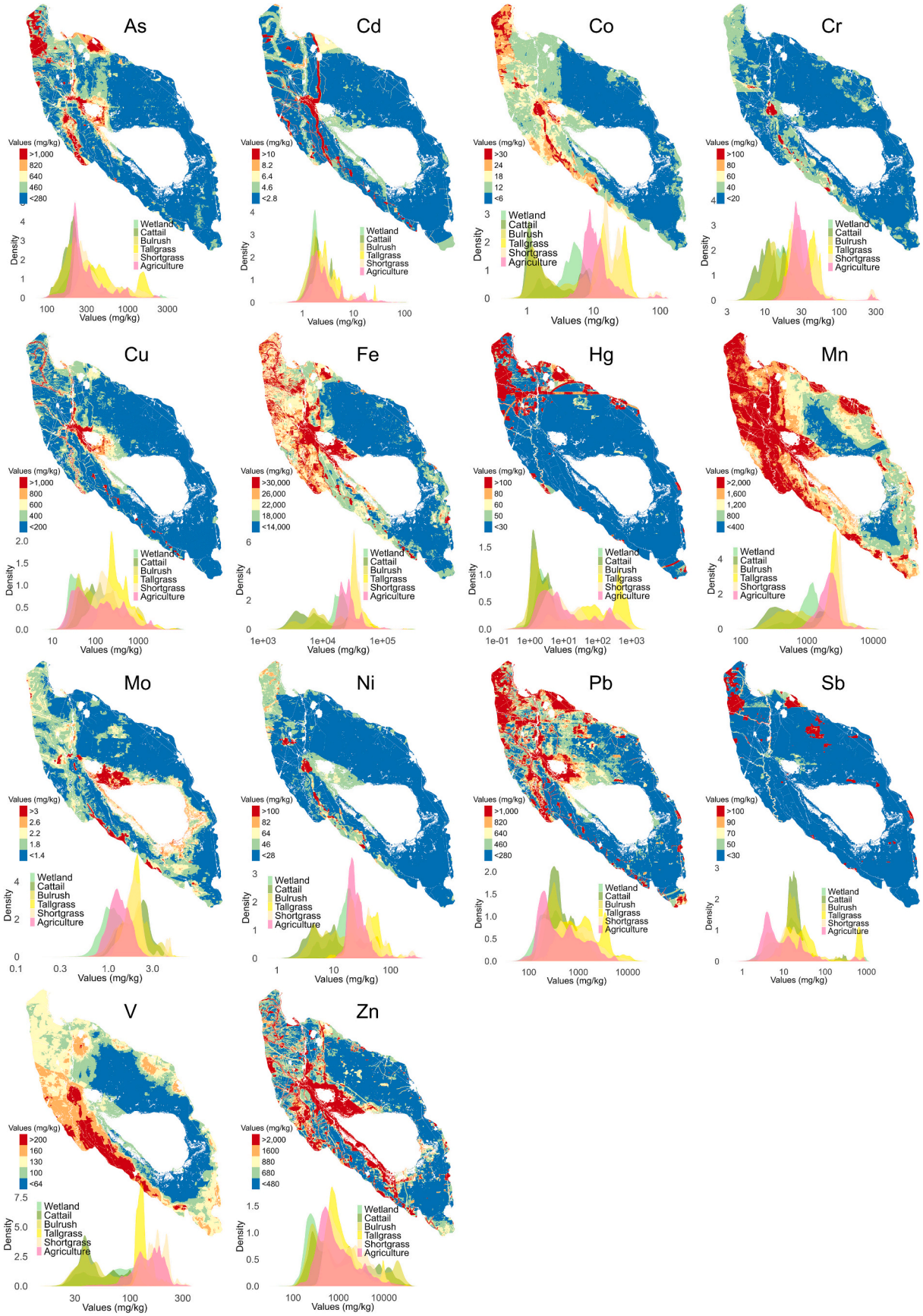

Fig. 6. Spatial distribution of heavy metals, metalloids, and trace elements in relation to vegetation cover types around Junin Lake.

Among heavy metals, Cd, Cu, Pb, and Zn exceed PEL reference values at multiple locations, with agricultural soils showing frequent exceedances. Mercury and nickel exhibit localized patterns, while chromium shows broader, homogeneous distribution below critical thresholds. Arsenic presents concerning patterns, reaching high concentrations in agricultural areas and exceeding TEL and PEL guidelines. Several elements (Cd, Hg, Mo) exhibit log-normal distributions with extreme values potentially exceeding ecological thresholds.

Trace elements Fe and Mn show widespread distributions reflecting lithogenic sources and sediment dynamics, while Mo and V concentrate primarily in agricultural and transitional zones. This spatially explicit assessment demonstrates that vegetation cover plays a fundamental role in controlling PTE distribution, supporting targeted monitoring in agricultural areas and conservation of natural vegetation systems for metal sequestration and watershed protection.

3.7. Ecological risk distribution

Fig. 7 presents the spatial distribution of three contamination assessment metrics mean contamination degree (mCD), pollution load index (PLI), and ecological risk index (RI) across the 74,940.6-ha study area surrounding Junin Lake. The mCD analysis reveals extensive contamination throughout the basin, with the most severe conditions concentrated in the central and southern sectors. The contamination classification shows 41.6 % of the area (31,188.6 ha) under extremely high contamination, 35.2 % (26,379.9 ha) under ultra-high contamination, and 22.7 % (17,021.4 ha) under very high contamination. Areas exhibiting moderate to low contamination levels occupy less than 1 % of the total area (349.5 ha), indicating the pervasive nature of environmental degradation.

The spatial distribution patterns of PLI and RI demonstrate strong concordance with mCD results. The PLI analysis indicates that nearly the entire study region exceeds established environmental quality thresholds, reflecting widespread and persistent anthropogenic contamination. Similarly, the RI assessment classifies most of the study area under very high ecological risk categories, indicating significant threats to ecosystem integrity from elevated concentrations of PTEs.

These findings reveal a critical environmental situation characterized by extensive contamination and elevated ecological vulnerability across the Junin Lake watershed. The spatial homogeneity of high contamination levels across multiple assessment indices underscores the severity and regional extent of environmental degradation. The results necessitate immediate implementation of comprehensive environmental management strategies, including contamination source control, remediation protocols, and ecosystem restoration measures to mitigate ongoing ecological risks and protect both environmental and human health.

3.8. Spatial distribution of non-carcinogenic (HI) and carcinogenic (TCR) risk in adults and children

Fig. 8 illustrates the spatial distribution of non-carcinogenic health risks (hazard index, HI) for seven PTEs in the Junin Lake watershed, with separate assessments for adult and pediatric populations. Risk levels were categorized as either no significant risk (HI < 1) or possible chronic adverse effects (HI ≥ 1).

The spatial analysis revealed pronounced age-dependent risk patterns. In the adult population, arsenic emerged as the predominant health concern, with 85.28 % of the study area exceeding the non-carcinogenic threshold (HI ≥ 1). Lead and mercury also demonstrated substantial risk coverage, affecting 30.50 % and 24.37 % of the assessed area, respectively. In contrast, cadmium, chromium, cobalt, and nickel exhibited minimal health risks, with over 99 % of the study area maintaining HI values below the threshold for chronic adverse effects.

Pediatric populations demonstrated considerably lower overall risk exposure. Arsenic remained the primary contaminant of concern, though its risk coverage was substantially reduced to 33.26 % of the study area. Mercury posed elevated risk across 10.75 % of the region, while the remaining elements (Cd, Cr, Co, Ni, and Pb) showed negligible risk potential, with nearly the entire study area falling within acceptable exposure limits.

These findings underscore significant age-related vulnerability differences in chronic exposure scenarios, with adult populations experiencing disproportionately higher health risks, particularly from arsenic, lead, and mercury contamination. The reduced risk profile in children may reflect different exposure pathways, physiological factors, or the conservative nature of pediatric risk assessment parameters.

Fig. 9 presents the spatial distribution of Target Cancer Risk (TCR) for six PTEs (As, Cd, Cr, Ni, Pb, Co) across adult and pediatric populations. Risk classifications follow established regulatory thresholds: no

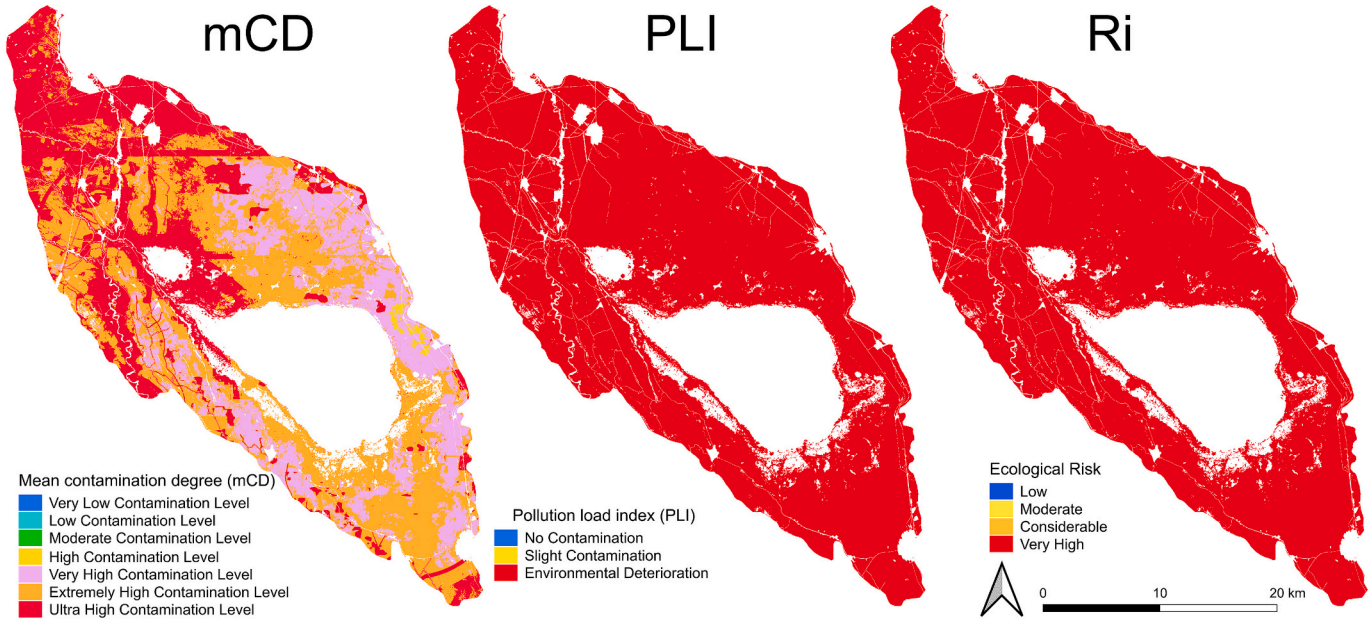

Fig. 7. Spatial distribution of contamination (mCD), pollution load (PLI), and ecological risk (RI) indices for PTEs around Junin Lake.

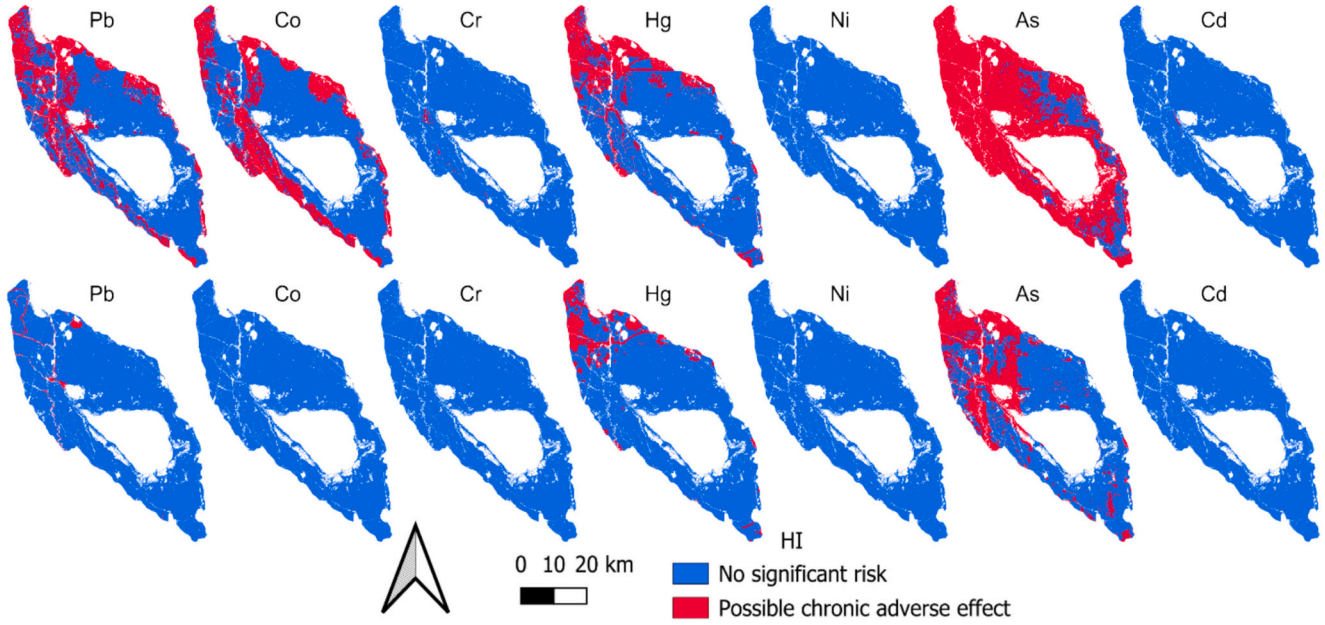

Fig. 8. Spatial distribution of non-carcinogenic risk (HI) due to exposure to PTEs in adults (top) and children (bottom) in the surroundings of Junin Lake.

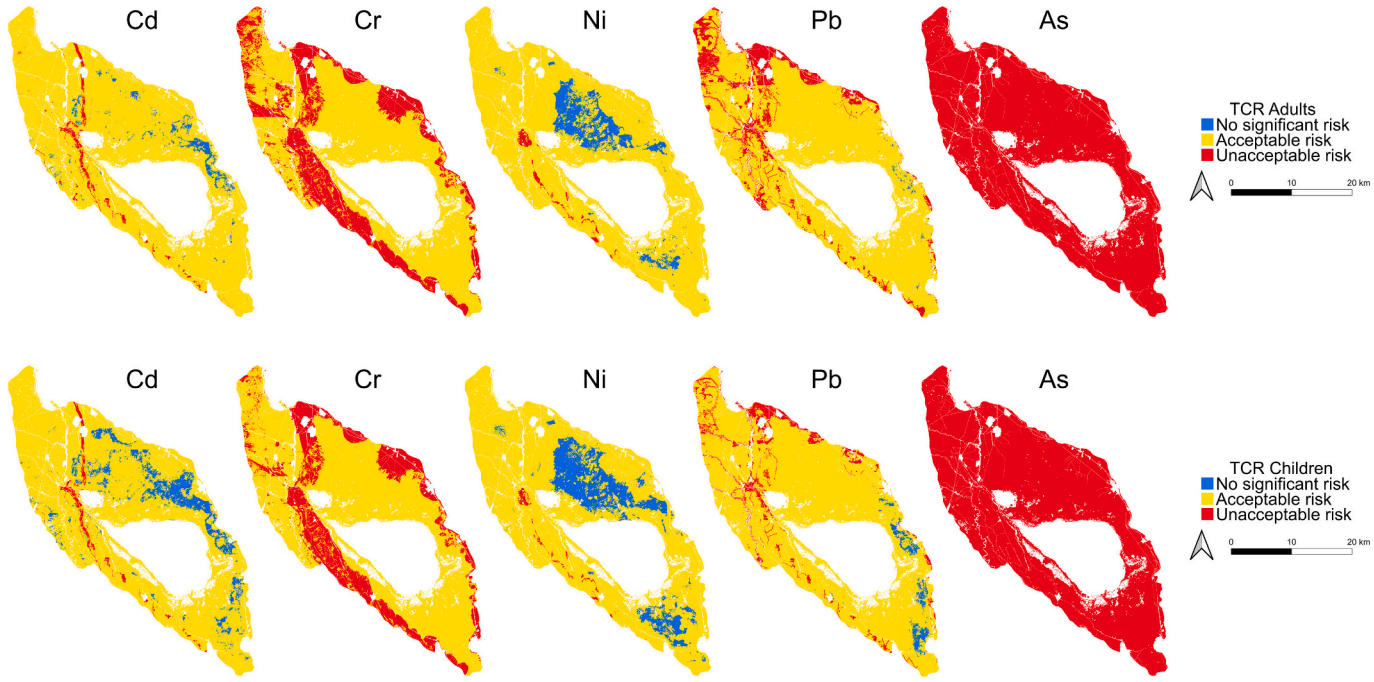

Fig. 9. Spatial distribution of carcinogenic risk (TCR) due to exposure to PTEs in adults and children in the surroundings of Junin Lake.

significant risk (TCR $< 1 \times 10^{-6}$), acceptable risk ($1 \times 10^{-6} \leq$ TCR $< 1 \times 10^{-4}$), and unacceptable risk (TCR $\geq 1 \times 10^{-4}$).

The adult population faces substantial carcinogenic exposure, with arsenic representing the most severe threat across the entire study area (100 % unacceptable risk). Chromium emerges as the second major contributor to regional cancer risk, with 30.09 % of the area classified as unacceptable. Lead presents a heterogeneous risk distribution, where 14.42 % of the area exceeds acceptable limits while the majority (85.35 %) remains within acceptable bounds. Cadmium and nickel demonstrate more favorable risk profiles, with 94.49 % and 89.36 % of areas maintaining acceptable risk levels, respectively, though localized contamination hotspots persist above regulatory thresholds.

Children exhibit comparatively lower carcinogenic risk exposure across most elements, reflecting age-specific exposure parameters and physiological differences. However, arsenic contamination remains universally problematic, with 100 % of the study area classified as unacceptable risk for pediatric populations. Other elements show markedly improved risk profiles: cadmium and nickel display substantial areas of no significant risk (24.38 % and 25.74 %, respectively), lead demonstrates minimal high-risk zones (0.01 % unacceptable, 3.86 % no significant risk), and chromium affects only 0.87 % of the area at high-risk levels.

The comparative analysis reveals age-dependent vulnerability patterns, with adults experiencing more severe carcinogenic risks due to prolonged exposure duration and higher contaminant intake rates. The total arsenic contamination across both demographic groups represents

a critical public health emergency requiring immediate intervention through comprehensive exposure mitigation strategies, targeted site remediation efforts, and coordinated public health interventions.

4. Discussions

4.1. Ecological risk and landscape vulnerability

The ecological risk assessment of the Junín Lake watershed reveals critical contamination by PTEs, with ecological risk index (RI) values substantially exceeding thresholds for very high risk. This contamination is most pronounced in agricultural zones and degraded highland grasslands, indicating strong anthropogenic influences on ecosystem integrity. These findings align with regional studies across the Andean highlands, where Custodio et al. (2021, 2023) documented similarly elevated ecological risks in central Peruvian river sediments, primarily attributed to agricultural runoff and urbanization. Comparable patterns emerge from Ecuador, where Beltrán-Dávalos et al. (2025) identified heightened ecological risks in unprotected Andean lakes, driven by anthropogenic enrichment of lead and copper.

The dominance of As and Pb in both mean contamination degree (mCD) and RI indices observed in this study mirrors findings from other Andean wetland systems. Custodio et al. (2022) similarly identified these elements as primary contributors to ecological risk in natural wetlands, while Aris (2017) documented concurrent declines in ecosystem services across high Andean wetlands due to mining expansion and intensive agriculture. The spatial concordance between degraded wetland zones and elevated contamination in Junín Lake reflects this broader regional trend of anthropogenic pressure on fragile highland mountain ecosystems.

These consistent patterns across the Andean region underscore the systematic nature of PTE contamination in high-altitude ecosystems and highlight the urgent need for integrated conservation and remediation strategies specifically tailored to montane environments.

4.2. Human health risk from PTE exposure

Spatial analysis reveals significant chronic health risks from PTE exposure, with agricultural and rural communities facing disproportionate hazards through multiple exposure pathways including ingestion, inhalation, and dermal contact. These findings contribute to growing evidence of PTE-related health risks in developing regions, where children consistently emerge as the most vulnerable demographic.

Although children are generally considered more vulnerable to heavy metal exposure due to their lower body weight, our findings indicate higher health risks for adults. This discrepancy can be attributed to longer exposure duration, increased frequency of contact, greater exposed skin surface, and prolonged inhalation of contaminated dust, particularly in agricultural and rural settings such as the surroundings of Lake Junín. Similar patterns have been reported in other mining-affected regions. For instance Zhuang et al. (2014) observed elevated risk levels among adults in the Dabaoshan area of China, largely due to continuous consumption of contaminated food and frequent contact with agricultural soils. Likewise, Li et al. (2022) highlighted that long-term exposure in adults significantly increased cumulative risk in mining-impacted farmlands.

Regarding the contribution of mining activities to the observed health risks, several studies have documented that both active operations and mining environmental liabilities (MELs) are major sources of toxic elements such as As, Pb, Cd, Zn, and Cu in high Andean soils. In regions like Junín, these contaminants are often linked to tailings leachate, abandoned waste, and poorly managed historical emissions (Cruzado-Tafur et al., 2020; Mendoza et al., 2020; Sun et al., 2017).

Recent global assessments reinforce these concerns. Siddig et al. (2025b) identified carcinogenic risks from chromium, nickel, cadmium, and arsenic across more than 70 % of surveyed land uses in Sudan, with children showing heightened vulnerability. Similarly, Haque et al. (2025) documented unacceptable risks from As, Cr, and Cd in urban and industrial settings, emphasizing indoor dust as a critical exposure vector. The dietary pathway also presents substantial risks, as demonstrated by Effiong et al. (2023), who identified As and Cd in processed foods as primary contributors to cancer risk in Nigeria.

Within the Andean context, Custodio et al. (2020) reported hazard index (HI) values exceeding unity for arsenic and lead in surface waters near Peruvian mining zones, with children's cancer risk classified as moderate to high. This pattern extends globally, with elevated HI and total cancer risk (TCR) values for As, Cd, Cr, and Ni documented across diverse geographic contexts, including China (Liu et al., 2024), Bangladesh (Jewel et al., 2024), Iran (Niknejad et al., 2024), and Nigeria (Taiwo et al., 2024).

The consistency of these findings across different continents and exposure scenarios validates our results and emphasizes the universal vulnerability of children to PTE exposure, reinforcing the critical need for targeted risk assessment and intervention strategies in contaminated environments.

4.3. Environmental covariates and predictive modeling

Effective PTE risk assessment requires integrated approaches that combine environmental covariates, vegetation characteristics, and advanced modeling techniques to capture the complex spatial variability of contamination. The observed variation in PTE levels across land cover types reflects differential retention capacities, with less disturbed environments such as wetlands and native grasslands typically exhibiting higher accumulation rates (Aduko et al., 2025).

Vegetation plays a multifaceted role in PTE dynamics, influencing both retention and mobility while serving as a natural barrier against erosion and contaminant dispersion (Carbajal et al., 2024; González Henao and Ghneim-Herrera, 2021; Pająk et al., 2018). The integration of multivariate environmental covariates including soil pH, texture, normalized difference vegetation index (NDVI), and elevation has proven essential for explaining metal distribution patterns, particularly in topographically complex montane regions (Adhikari et al., 2024; Rahaman et al., 2025).

ML algorithms, particularly RF models, have demonstrated superior performance in handling the nonlinear relationships and multicollinearity inherent in environmental datasets (Li et al., 2025b; Su et al., 2024; Xu et al., 2024). The integration of remote sensing data with ML approaches further enhances predictive mapping capabilities, proving especially valuable in data-sparse regions where traditional sampling approaches are logistically challenging (Guo et al., 2023; Khosravi et al., 2021).

This methodological framework validates our approach of utilizing vegetation indices as ecological indicators and environmental covariates as predictors, thereby improving both spatial resolution and accuracy of PTE risk assessment in sensitive Andean ecosystems.

4.4. Management implications

The convergent evidence from ecological risk assessment and human health evaluation underscores the critical need for comprehensive environmental management strategies that simultaneously address ecosystem integrity and public health protection. The persistent contamination by arsenic, lead, and mercury, coupled with disproportionate risks to vulnerable populations particularly children demands immediate and sustained intervention (Hsieh et al., 2014; Rodríguez et al., 2024).

Effective management requires a multi-pronged approach encompassing adaptive land use planning that considers contamination patterns and exposure pathways, implementation of improved agricultural practices that minimize PTE mobilization, and establishment of

community-based monitoring programs that engage local stakeholders in ongoing risk assessment. Additionally, targeted remediation efforts should prioritize areas with the highest combined ecological and human health risks, while considering the unique challenges posed by high-altitude environments (J. Liu et al., 2018).

The broader applicability of these findings to similar highland systems throughout the Andes suggests that regional coordination and knowledge sharing could enhance the effectiveness of management interventions. Ultimately, protecting both environmental integrity and public health in the Junín watershed and comparable montane ecosystems requires sustained commitment to evidence-based management practices that integrate scientific understanding with community needs and environmental justice considerations (Nassar and Khater, 2023).

5. Conclusion

This assessment reveals critical contamination by PTEs in the Junín Lake watershed, with arsenic, lead, cadmium, and zinc concentrations substantially exceeding ecological and human health thresholds. Nearly the entire study area faces very high ecological risk, while local populations experience unacceptable carcinogenic risks, particularly from arsenic exposure. The integration of remote sensing, ML, and land cover analysis effectively identified contamination hotspots across this heterogeneous land cover formations, demonstrating significant potential for application in similar regions.

The convergent evidence demands urgent coordinated intervention strategies including immediate soil and water remediation, adaptive land use policies restricting PTE-mobilizing activities, and community-based monitoring programs. These findings likely reflect broader contamination patterns across Andean montane basins, indicating the need for regional policy coordination and sustained investment in high-altitude ecosystem protection. The preservation of Junín Lake's ecological integrity and community health represents a critical test of environmental justice commitments, requiring rapid translation of scientific findings into concrete policy action.

CRediT authorship contribution statement

Samuel Pizarro: Writing – review & editing, Visualization, Software, Formal analysis, Data curation, Conceptualization. **Edilson Requena-Rojas:** Writing – original draft, Visualization, Software, Methodology. **Elgar Barboza:** Visualization, Validation, Software, Methodology. **Eunice Peña-Elme:** Writing – review & editing, Validation, Methodology. **Alberto Arias-Arredondo:** Validation, Software, Methodology, Formal analysis, Data curation. **Dennis Ccopi:** Writing – review & editing, Visualization, Software, Methodology, Investigation, Formal analysis, Conceptualization.

Ethics statement

Not applicable: this manuscript does not include human or animal research.

Funding

This research was funded by the INIA project "Mejoramiento de los servicios de investigación y transferencia tecnológica en el manejo y recuperación de suelos agrícolas degradados y aguas para riego en la pequeña y mediana agricultura en los departamentos de Lima, Áncash, San Martín, Cajamarca, Lambayeque, Junín, Ayacucho, Arequipa, Puno y Ucayali" CUI 2487112, of the Ministry of Agrarian Development and Irrigation (MIDAGRI) of the Peruvian Government. We would like to express our deepest gratitude to everyone who contributed to this research at the Santa Ana Experimental Station – Huancayo.

Declaration of competing interest

The authors declare that they have no known competing financial interests or personal relationships that could have appeared to influence the work reported in this paper.

Appendix A. Supplementary data

Supplementary data to this article can be found online at https://doi.org/10.1016/j.scitotenv.2025.180327.

Data availability

Data will be made available on request.

References

Adhikari, K., Mancini, M., Libohova, Z., Blackstock, J., Winzeler, E., Smith, D.R., Owens, P.R., Silva, S.H.G., Curi, N., 2024. Heavy metals concentration in soils across the conterminous USA: spatial prediction, model uncertainty, and influencing factors. Sci. Total Environ. 919. https://doi.org/10.1016/j.scitotenv.2024.170972.

Aduko, J., Yakubu, M.A., Anokye, K., 2025. Assessing the environmental impacts of urban sprawl on vegetation cover and ecosystem integrity in Wa municipality, Ghana. World Dev. Sustain. 6, 100225. https://doi.org/10.1016/j.wds.2025.100225.

Agyeman, P.C., Khosravi, V., Michael Kebonye, N., John, K., Borůvka, L., Vašát, R., 2022. Using spectral indices and terrain attribute datasets and their combination in the prediction of cadmium content in agricultural soil. Comput. Electron. Agric. 198, 107077. https://doi.org/10.1016/J.COMPAG.2022.107077.

Ahmad, Z., Khan, S.M., Ullah, A., Afza, R., Yang, J., 2025. Source apportionment, carcinogenic and non-carcinogenic risks assessment of soil heavy metals in marble waste polluted environment; role of vegetation in risk mitigation. J. Hazard. Mater. Adv. 18, 100689. https://doi.org/10.1016/J.HAZADV.2025.100689.

Aris, I.D., 2017. Ecological assessment of high Andean wetlands and environmental offset measures in mining activities. https://www.researchgate.net/publication/344482759.

Beltrán-Dávalos, A.A., Salazar, C., Kurbatova, A.I., Echeverría, M., Merino, A., Otero, X. L., 2025. Sediment chemistry and ecological risk assessment in Andean lakes of Central Ecuador: influence of trophic status on accumulation patterns. Sustainability 17 (8). https://doi.org/10.3390/su17083397.

Caicedo-Rivas, G., Salas-Moreno, M., Marrugo-Negrete, J., 2023. Health risk assessment for human exposure to heavy metals via food consumption in inhabitants of Middle Basin of the Atrato River in the Colombian Pacific. Int. J. Environ. Res. Public Health 20 (1). https://doi.org/10.3390/ijerph20010435.

Cano, D., Pizarro, S., Cacciuttolo, C., Peñaloza, R., Yaranga, R., Gandini, M.L., 2023. Study of ecosystem degradation dynamics in the Peruvian highlands: Landsat time-series trend analysis (1985–2022) with ARVI for different vegetation cover types. Sustainability (Switzerland) 15 (21). https://doi.org/10.3390/su152115472.

Carbajal, M., Ramírez, D.A., Turin, C., Schaeffer, S.M., Konkel, J., Ninanya, J., Rinza, J., De Mendiburu, F., Zorogastua, P., Villaorduñ, L., Quiroz, R., 2024. From rangelands to cropland, land-use change and its impact on soil organic carbon variables in a Peruvian Andean highlands: a machine learning modeling approach. Ciudad Saber 12, 15024. https://doi.org/10.1007/s10021-024-0092.

Cruzado-Tafur, E., Torró, L., Bierla, K., Szpunar, J., & Tauler, E. (2020). Heavy metal contents in soils and native flora inventory at mining environmental liabilities in the Peruvian Andes.

Cruzado-Tafur, E., Torró, L., Bierla, K., Szpunar, J., Tauler, E., 2021. Heavy metal contents in soils and native flora inventory at mining environmental liabilities in the Peruvian Andes. J. S. Am. Earth Sci. 106, 103107. https://doi.org/10.1016/J.JSAMES.2020.103107.

Cui, W., Mei, Y., Liu, S., Zhang, X., 2023. Health risk assessment of heavy metal pollution and its sources in agricultural soils near Hongfeng Lake in the mining area of Guizhou Province, China. Front. Public Health 11. https://doi.org/10.3389/fpubh.2023.1276925.

Cusiche, L., Miranda, G., 2019. Contaminación por aguas residuales e indicadores de calidad en la reserva nacional 'Lago Junín', Perú. Rev. Mex. Cienc. Agríc. 10 (6).

Cusiche Pérez, L.F., 2017. Ecodiseño para mitigar la contaminación por aguas residuales al lago de Junín. Universidad Nacional Del Centro Del Perú.

Custodio, M., Cuadrado, W., Peñaloza, R., Montalvo, R., Ochoa, S., Quispe, J., 2020. Human risk from exposure to heavy metals and arsenic in water from rivers with mining influence in the Central Andes of Peru. Water 12 (7). https://doi.org/10.3390/w12071946.

Custodio, M., Fow, A., Chanamé, F., Orellana-Mendoza, E., Peñaloza, R., Alvarado, J.C., Cano, D., Pizarro, S., 2021. Ecological risk due to heavy metal contamination in sediment and water of natural wetlands with tourist influence in the central region of Peru. Water 13 (16). https://doi.org/10.3390/w13162256.

Custodio, M., Espinoza, C., Orellana, E., Chanamé, F., Fow, A., Peñaloza, R., 2022. Assessment of toxic metal contamination, distribution and risk in the sediments from lagoons used for fish farming in the central region of Peru. Toxicol. Rep. 9 (3909), 1603–1613. https://doi.org/10.1016/j.toxrep.2022.07.016.

Custodio, M., Fow, A., De la Cruz, H., Chanamé, F., Huarcaya, J., 2023. Potential ecological risk from heavy metals in surface sediment of lotic systems in central region Peru. Front. Water 5. https://doi.org/10.3389/frwa.2023.1295712.
Custodio, V.M., Chanamé, Z.F., Bulege, G.W., 2019. Evaluación de la calidad del agua del río Cunas índices fisicoquimicos y biologicos, Junìn - Perú. Prospect. Univ. 10 (1), 98–105. https://doi.org/10.26490/uncp.prospectivauniversitaria.2013.10.26.
Duman, M., Eronat, A.H., Talas, E., Gerdanlı, M.C., Tükel, C., 2025. Understanding heavy metal pollution dynamics in Çandarlı Gulf, western Türkiye: insights from spatial analysis, sediment transport modeling and ecological risk assessment. Cont. Shelf Res. 285, 105393. https://doi.org/10.1016/J.CSR.2024.105393.
Effiong, E.A., Ezejiofor, A.N., Ekhator, O.C., Bocca, B., Battistini, B., Ruggieri, F., Frazzoli, C., Orisakwe, O.E., 2023. Probabilistic non-carcinogenic and carcinogenic risk assessments of potential toxic metals (PTMs) and polycyclic aromatic hydrocarbons (PAHs) in canned foods in Nigeria: understanding the size of the problem. J. Trace Elem. Miner. 4, 100069. https://doi.org/10.1016/j.jtemin.2023.100069.
EPA, 1996. Soil Screening Guidance: User's Guide, Second edition https://rais.ornl.gov/documents/SSG_nonrad_user.pdf?utm_source.
EPA Method 3050B, 1996. Acid Digestion of Sediments, Sludges, and Soils 3050b.
EPA Method 6010D, 2018. Inductively Coupled Plasma—Optical Emission Spectrometry 6010D.
Ettler, V., 2016. Soil contamination near non-ferrous metal smelters: a review. Appl. Geochem. 64, 56–74. https://doi.org/10.1016/J.APGEOCHEM.2015.09.020.
FAO (Food and Agriculture Organization of the United Nations), 2000. Assessing Soil Contamination: A Reference Manual.
Fu, T., Song, H., Yang, B., Liu, R., 2025. Evaluation of heavy metal accumulation and pollution in soils from the vanadium-titanium magnetite mining region in Panzhihua, China. Ore Geol. Rev., 100098 https://doi.org/10.1016/J.OREOA.2025.100098.
Gan, L., Wang, J., Xie, M., Yang, B., 2022. Ecological risk and health risk analysis of soil potentially toxic elements from oil production plants in central China. Sci. Rep. 12 (1). https://doi.org/10.1038/s41598-022-21629-y.
González Henao, S., Ghneim-Herrera, T., 2021. Heavy metals in soils and the remediation potential of bacteria associated with the plant microbiome. Front. Environ. Sci. https://doi.org/10.3389/fenvs.2021.604216.
Gorelick, N., Hancher, M., Dixon, M., Ilyushchenko, S., Thau, D., Moore, R., 2017. Google Earth Engine: planetary-scale geospatial analysis for everyone. Remote Sens. Environ. 202, 18–27. https://doi.org/10.1016/j.rse.2017.06.031.
Guo, B., Ren, P., Wang, L., Li, S., Luo, C., Zhao, Y., Zhao, H., Sun, J., Ji, P., 2024. Material flow analysis of heavy metals in large-scale cattle farms and ecological risk assessment of cattle manure application to fields. J. Environ. Manag. 364, 121452. https://doi.org/10.1016/J.JENVMAN.2024.121452.
Guo, X., Bian, Z., Wang, S., Wang, Q., Zhang, Y., Zhou, J., Lin, L., 2020. Prediction of the spatial distribution of soil arthropods using a random forest model: a case study in Changtu County, Northeast China. Agric. Ecosyst. Environ. 292, 106818. https://doi.org/10.1016/J.AGEE.2020.106818.
Guo, Y., Sun, Y., Fan, D., Wang, S., Agathokleous, E., Zhu, Y., Han, J., 2023. New insights into the role of soil properties in driving cadmium-induced hormesis in soil alkaline phosphatase under vegetation cover change. Sci. Total Environ. 892. https://doi.org/10.1016/j.scitotenv.2023.164798.
Hakanson, L., 1980. An ecological risk index for aquatic pollution control. A sedimentological approach. Water Res. 14 (8), 975–1001. https://doi.org/10.1016/0043-1354(80)90143-8.
Haque, M.R., Ahmed, W., Haque, A., Rayhan, M.R.I., Moniruzzaman, M., Akbor, M.A., Shammi, M., Rahman, M.M., 2025. Unveiling the hidden threat: a multi-faceted assessment of heavy metal contamination in indoor dust along with ecological risk and human health implications. J. Hazard. Mater. Adv. 18. https://doi.org/10.1016/j.hazadv.2025.100644.
Hoang, H.G., Hadi, M., Nguyen, M.K., Hai Nguyen, N.S., Huy Le, P.Q., Nguyen, K.N., Tran, H.T., Mishra, U., 2025. Assessing heavy metal pollution levels and associated ecological risks in peatland areas in the Mekong Delta region. Environ. Res. 274, 121319. https://doi.org/10.1016/J.ENVRES.2025.121319.
Hsieh, R.-L., Huang, Y.-L., Shiue, H.-S., Huang, S.-R., Lin, M.-I., Mu, S.-C., Chung, C.-J., Hsueh, Y.-M., 2014. Arsenic methylation capacity and developmental delay in preschool children in Taiwan. Int. J. Hyg. Environ. Health 217 (6), 678–686. https://doi.org/10.1016/j.ijheh.2014.02.004.
Hu, X., Zhai, X., Jin, Y., Wade, T.L., Zhou, X., Zhuang, T., Ning, J., Song, X., Cai, W., Chen, Z., Li, X., 2024. Ecological risk assessment of dissolved heavy metals in the Yangtze River estuary and Zhejiang coastal waters, China. Mar. Pollut. Bull. 205, 116570. https://doi.org/10.1016/J.MARPOLBUL.2024.116570.
Hui, X., Li, A., Chang, S., Wang, A., Wang, L., Li, C., 2025. Concentrations and human health risks attributed to potentially toxic elements (PTEs) in water resources in China: systematic review and meta-analysis. Ecotoxicol. Environ. Saf. 291, 117801. https://doi.org/10.1016/J.ECOENV.2025.117801.
Jewel, M.A.S., Zinat, A., Khatun, B., Akter, S., Barman, A.C., Satter, A., Haque, M.A., 2024. Ecological and public health risk assessment of potentially toxic elements in the surface sediments of the Pasur river estuary, Bangladesh. Heliyon 10 (8), e29278. https://doi.org/10.1016/j.heliyon.2024.e29278.
Kasraei, B., Schmidt, M.G., Zhang, J., Bulmer, C.E., Filatow, D.S., Arbor, A., Pennell, T., Heung, B., 2024. A framework for optimizing environmental covariates to support model interpretability in digital soil mapping. Geoderma 445, 116873. https://doi.org/10.1016/J.GEODERMA.2024.116873.
Khoshakhlagh, A.H., Ghobakhloo, S., Gruszecka-Kosowska, A., 2024. Inhalational exposure to heavy metals: carcinogenic and non-carcinogenic risk assessment. J. Hazard. Mater. Adv. 16, 100485. https://doi.org/10.1016/J.HAZADV.2024.100485.
Khosravi, V., Doulati Ardejani, F., Gholizadeh, A., Saberioon, M., 2021. Satellite imagery for monitoring and mapping soil chromium pollution in a mine waste dump. Remote Sens. 13 (7). https://doi.org/10.3390/rs13071277.
Kong, Y., Liu, J., Pan, J., Ruan, X., Wang, Y., 2025. Migration characteristics and health risk assessment of heavy metals in soil-vegetable system in a typical wastewater irrigation area. J. Food Compos. Anal. 143, 107564. https://doi.org/10.1016/J.JFCA.2025.107564.
Kuhn, M., 2008. Building predictive models in *R* using the caret package. J. Stat. Softw. 28 (5). https://doi.org/10.18637/jss.v028.i05.
Lê, S., Josse, J., Rennes, A., Husson, F., 2008. Factominer: an R package for multivariate analysis. J. Stat. Softw. 25. http://www.jstatsoft.org/.
Li, R., Wang, Z., Li, Y., Wu, T., 2025a. Regional ecological risk assessment and transfer mechanism based on improved gravity and social network analysis model: a case study of Northwest China. Ecol. Indic. 172, 113243. https://doi.org/10.1016/J.ECOLIND.2025.113243.
Li, Yan, Xiang, B., Wang, T., He, Y., Liu, X., Li, Y., Ren, S., Wang, E., Guo, G., 2025b. Applications of machine learning in potentially toxic elemental contamination in soils: a review. Ecotoxicol. Environ. Saf. https://doi.org/10.1016/j.ecoenv.2025.118110.
Li, Yan, Yu, Y., Ding, S., Dai, W., Shi, R., Cui, G., Li, X., 2025c. Application of machine learning in soil heavy metals pollution assessment in the southeastern Tibetan plateau. Sci. Rep. 15 (1). https://doi.org/10.1038/s41598-025-97006-2.
Li, Yanhua, Zhu, Q., Tang, X., Wang, C., Zhai, S., 2022. Ecological and health risk assessment of heavy metals in farmland in the south of Zhangbei County, Hebei Province, China. Appl. Sci. 12 (23). https://doi.org/10.3390/app122312425.
Liaw, A., Wiener, M., 2002. Classification and regression by randomForest (Vol. 2, Number 3). http://www.stat.berkeley.edu/.
Lima, G. dos S., Suarez, C.A., Gemeiner, H., Serafini, P.P., de Deus, J.P.A., Viana, J.L.M., Menegario, A.A., 2025. Potentially toxic elements (PTEs) in seabirds foraging across a heterogeneous landscape: cross-species bioaccumulation patterns. Environ. Pollut. 367 (December 2024), 125609. https://doi.org/10.1016/J.ENVPOL.2024.125609.
Liu, J., Wang, Z., Zhao, H., Peros, M., Yang, Q., Liu, S., Li, H., Wang, S., Bu, Z., 2018. Mercury and arsenic in the surface peat soils of the Changbai Mountains, northeastern China: distribution, environmental controls, sources, and ecological risk assessment. Environ. Sci. Pollut. Res. 25 (34), 34595–34609. https://doi.org/10.1007/s11356-018-3380-5.
Liu, Y., Kuang, W., Sun, X., Wang, W., Lin, C., Lin, H., 2024. Fractionation, spatial distribution, ecological and health risk assessment of cobalt and nickel in surface sediment of a bay along the southeast coast of China. Mar. Pollut. Bull. 206. https://doi.org/10.1016/j.marpolbul.2024.116786.
Lovynska, V., Bayat, B., Bol, R., Moradi, S., Rahmati, M., Raj, R., Sytnyk, S., Wiche, O., Wu, B., Montzka, C., 2024. Monitoring heavy metals and metalloids in soils and vegetation by remote sensing: a review. Remote Sens. 16 (17), 3221. https://doi.org/10.3390/rs16173221.
Ma, X., Wang, J., Zhou, K., Zhang, W., Chen, A., 2025. Uncertainty in soil elemental prediction using machine learning and hyperspectral remote sensing. J. Hazard. Mater., 138502 https://doi.org/10.1016/J.JHAZMAT.2025.138502.
Martin, A.J., McNee, J.J., Pedersen, T.F., 2001. The reactivity of sediments impacted by metal-mining in Lago Junin, Peru. J. Geochem. Explor. 74 (1–3), 175–187. https://doi.org/10.1016/S0375-6742(01)00183-2.
Mendoza, E.O., Custodio, M., Ascensión, J., Bastos, M.C., 2020. Heavy metals in soils from high Andean zones and potential ecological risk assessment in Peru's Central Andes. J. Ecol. Eng. 21 (8), 108–119. https://doi.org/10.12911/22998993/127094.
Ministerio del Ambiente, 2015. Mapa Nacional de Cobertura Vegetal — Memoria Descriptiva. https://www.gob.pe/institucion/minam/informes-publicaciones/2674-mapa-nacional-de-cobertura-vegetal-memoria-descriptiva.
Mohammadi, M.J., Farhadi, M., Ghanbari, S., Asban, P., Kiani, F., Taherian, M., Mir, I., 2023. Ecological risk assessment of heavy metals in urban dust in Iran: a systematic review and meta-analysis. Toxicol. Rep. 11, 471–480. https://doi.org/10.1016/J.TOXREP.2023.11.007.
Moreno-Aguirre, S.B., Vértiz-Osores, J.J., Paredes-Espinal, C.E., Meseth, E., Vílchez-Ochoa, G.L., Espino-Ciudad, J.A., Flores del Pino, L., 2024. Ecological risk of metals in Andean water resources: a framework for early environmental assessment of mining projects in Peru. Heliyon 10 (9), e30739. https://doi.org/10.1016/J.HELIYON.2024.E30739.
Moura-Bueno, J.M., Dalmolin, R.S.D., Horst-Heinen, T.Z., Grunwald, S., ten Caten, A., 2021. Environmental covariates improve the spectral predictions of organic carbon in subtropical soils in southern Brazil. Geoderma 393, 114981. https://doi.org/10.1016/J.GEODERMA.2021.114981.
Nassar, S.E., Khater, Z.Z., 2023. Arsenic and mercury concentrations, ecological and health risk assessment in freshwater sediment and *Oreochromis niloticus* (Linnaeus, 1758) in a River Nile Canal, Egypt. Egypt. J. Aquat. Biol. Fish. 27 (4), 467–482. https://doi.org/10.21608/ejabf.2023.311149.
Nawrot, N., Wojciechowska, E., Mohsin, M., Kuittinen, S., Pappinen, A., Rezania, S., 2021. Trace metal contamination of bottom sediments: a review of assessment measures and geochemical background determination methods. Minerals 11 (8), 872. https://doi.org/10.3390/min11080872.
Niknejad, H., Esbakian Bandpei, B., Abedi Sarvestani, R., Mohseni-Bandpei, A., Saeedi, R., Abtahi, M., Gholami-Borujeni, F., 2024. Probabilistic health risk assessment of heavy metals in rice produced in Mazandaran province, Iran. J. Food Compos. Anal. 128, 106068. https://doi.org/10.1016/j.jfca.2024.106068.
Paes, É.C., Veloso, G.V., da Fonseca, A.A., Fernandes-Filho, E.I., Fontes, M.P.F., Soares, E.M.B., 2022. Predictive modeling of contents of potentially toxic elements using morphometric data, proximal sensing, and chemical and physical properties of soils under mining influence. Sci. Total Environ. 817. https://doi.org/10.1016/j.scitotenv.2022.152972.

Pająk, M., Błońska, E., Szostak, M., Gąsiorek, M., Pietrzykowski, M., Urban, O., Derbis, P., 2018. Restoration of vegetation in relation to soil properties of spoil heap heavily contaminated with heavy metals. Water Air Soil Pollut. 229 (12). https://doi.org/10.1007/s11270-018-4040-6.

Pizarro, S.E., Pricope, N.G., Vargas-Machuca, D., Huanca, O., Ñaupari, J., 2022. Mapping land cover types for Highland Andean ecosystems in Peru using Google Earth Engine. Remote Sens. 14 (7). https://doi.org/10.3390/rs14071562.

R Core Team, 2021. R: A Language and Environment for Statistical Computing. In: R Foundation for Statistical Computing. Vienna, Austria. https://www.R-project.org/.

Rahaman, M., Southworth, J., Amanambu, A.C., Tefera, B.B., Alruzuq, A.R., Safaei, M., Hasan, M.M., Smith, A.C., 2025. Combining deep learning and machine learning techniques to track air pollution in relation to vegetation cover utilizing remotely sensed data. J. Environ. Manag. 376. https://doi.org/10.1016/j.jenvman.2025.124323.

Reimann, C., De Caritat, P., 2005. Distinguishing between natural and anthropogenic sources for elements in the environment: regional geochemical surveys versus enrichment factors. Sci. Total Environ. 337 (1–3), 91–107. https://doi.org/10.1016/J.SCITOTENV.2004.06.011.

Rodbell, D.T., Delman, E.M., Abbott, M.B., Besonen, M.T., Tapia, P.M., 2014. The heavy metal contamination of Lake Junín National Reserve, Peru: an unintended consequence of the juxtaposition of hydroelectricity and mining. GSA Today 4–10. https://doi.org/10.1130/GSATG200A.1.

Rodríguez, R., Garcia-Gonzalez, H., Hernández, Z., Sanmiquel, L., 2024. Tackling arsenic and mercury contamination: implications for sustainable mining and occupational health risks. Sustainability 16 (10), 4027. https://doi.org/10.3390/su16104027.

Safadoust, A., Khaleghi, S., Kolahchi, Z., 2025. Environmental risks of heavy metals in railway soils: challenges to ecosystem management. Sci. Total Environ. 974, 179217. https://doi.org/10.1016/J.SCITOTENV.2025.179217.

Salgado, L., López-Sánchez, C.A., Colina, A., Baragaño, D., Forján, R., Gallego, J.R., 2023. Hg and As pollution in the soil-plant system evaluated by combining multispectral UAV-RS, geochemical survey and machine learning. Environ. Pollut. 333, 122066. https://doi.org/10.1016/J.ENVPOL.2023.122066.

del Sante, S., Sotomayor, D.A., Mantas, A.I., Aramayo, A., Sosa, M., Caro, C., 2025. Water pollution and culturally perceived environmental pollution at the Peruvian highlands. Environ. Monit. Assess. 197 (5), 578. https://doi.org/10.1007/s10661-025-14016-3.

Shen, W., Hu, Y., Zhang, J., Zhao, F., Bian, P., Liu, Y., 2021. Spatial distribution and human health risk assessment of soil heavy metals based on sequential Gaussian simulation and positive matrix factorization model: a case study in irrigation area of the Yellow River. Ecotoxicol. Environ. Saf. 225, 112752. https://doi.org/10.1016/J.ECOENV.2021.112752.

Siddig, M.M.S., Asabere, S.B., Al-Farraj, A.S., Brevik, E.C., Sauer, D., 2025a. Pollution and ecological risk assessment of heavy metals in anthropogenically-affected soils of Sudan: a systematic review and meta-analysis. J. Hazard. Mater. Adv. 17, 100601. https://doi.org/10.1016/J.HAZADV.2025.100601.

Siddig, M.M.S., Brevik, E.C., Sauer, D., 2025b. Human health risk assessment from potentially toxic elements in the soils of Sudan: a meta-analysis. Sci. Total Environ. 958 (November 2024), 178196. https://doi.org/10.1016/j.scitotenv.2024.178196.

Spater, M.R., Montúfar, R., Luzuriaga, C.X., Cañellas-Boltà, N., Trapote, M. del C., Smedley, R., Marchant, R., Montoya, E., 2024. Vegetation response to Holocene hydroclimatic variability in the aseasonal forests of the North-Western Amazon. Palaeogeogr. Palaeoclimatol. Palaeoecol. 649. https://doi.org/10.1016/j.palaeo.2024.112303.

Su, Y., Yu, H., Gao, C., Sun, S., Liang, Y., Liu, G., Zhang, X., Dong, Y., Liu, X., Chen, G., Shao, H., McMinn, A., Wang, M., 2024. Effects of vegetation cover and aquaculture pollution on viral assemblages in mangroves sediments. J. Hazard. Mater. 476. https://doi.org/10.1016/j.jhazmat.2024.135147.

Sun, G., Li, Z., Liu, T., Chen, J., Wu, T., Feng, X., 2017. Metal exposure and associated health risk to human beings by street dust in a heavily industrialized city of Hunan province, Central China. Int. J. Environ. Res. Public Health 14 (3). https://doi.org/10.3390/ijerph14030261.

Sun, Y., Lei, S., Zhao, Y., Wei, C., Yang, X., Han, X., Li, Y., Xia, J., Cai, Z., 2024. Spatial distribution prediction of soil heavy metals based on sparse sampling and multi-source environmental data. J. Hazard. Mater. 465. https://doi.org/10.1016/j.jhazmat.2023.133114.

Taiwo, A.M., Akintunde, O.O., Gbadebo, A.M., Akinremi, C.A., 2024. Assessment of probable health risk of potentially toxic metals in irrigable wetland soils from Ogun and Lagos States, Southwestern Nigeria. J. Trace Elem. Miner. 9, 100179. https://doi.org/10.1016/j.jtemin.2024.100179.

Tan, K., Wang, H., Chen, L., Du, Q., Du, P., Pan, C., 2020. Estimation of the spatial distribution of heavy metal in agricultural soils using airborne hyperspectral imaging and random forest. J. Hazard. Mater. 382, 120987. https://doi.org/10.1016/J.JHAZMAT.2019.120987.

Tanwar, D., Tyagi, S., Sarma, K., 2025. Seasonal and spatial investigation of groundwater contamination of potential toxic elements (PTEs) and associated health risks of southern region of Delhi, India. Chemosphere 378, 144398. https://doi.org/10.1016/J.CHEMOSPHERE.2025.144398.

Taylor, S.R., Mclennan, S.M., 1995. The geochemical the continental evolution crust. Rev. Mineral. Geochem. 33 (2), 241–265.

Tiabou, A.F., Atabe, G.A.A., Sigue, C., Yiika, L.P., Kachoueiyan, F., Forchenallah, N.E., 2024. Appraisal of pollution, ecological and health risks assessment of trace metals in soils of Logbadjeck quarrying area, Nyong Series, Cameroon. J. Trace Elem. Miner. 10, 100204. https://doi.org/10.1016/j.jtemin.2024.100204.

Tomlinson, D.L., Wilson, J.G., Harris, C.R., Jeffrey, D.W., 1980. Problems in the assessment of heavy-metal levels in estuaries and the formation of a pollution index. Helgoländer Meeresun. 33.

Ullah, I., Adnan, M., Nawab, J., Safi, I., Khan, S., 2025. Occurrence, distribution and ecological health risk assessment of heavy metals through consumption of drinking water in urban, industrial, and mining areas of semi-arid to humid subtropical areas. J. Geochem. Explor. 275, 107786. https://doi.org/10.1016/J.GEXPLO.2025.107786.

US-EPA, 2004. Supplemental Guidance for Dermal Risk Assessment, Part E of Risk Assessment Guidance for Superfund, Human Health Evaluation Manual. http://www.epa.gov/oerrpage/superfund/programs/risk/ragse/.

Vasilachi, I.C., Stoleru, V., Gavrilescu, M., 2023. Analysis of heavy metal impacts on cereal crop growth and development in contaminated soils. Agriculture 13 (10). https://doi.org/10.3390/agriculture13101983.

Vasudhevan, P., Pu, S., Ayyamperumal, R., Manikandan, E., Sujitha, S.B., Singh, S., Ponniah, J.M., Dixit, S., Thangavel, P., 2025. Pollution assessment, ecological risk and source identification of heavy metals in paddy soils and rice grains from Salem, South India. J. Hazard. Mater. Adv. 17, 100526. https://doi.org/10.1016/J.HAZADV.2024.100526.

Victoria, A., Cobbina, S.J., Boakye Dampare, S., Duwiejuah, A.B., Dampare, S.B., Ballu, A., 2014. Heavy metals concentration in road dust in the Bolgatanga municipality, Ghana. J. Environ. Pollut. Hum. Health 2 (4), 74–80. https://doi.org/10.12691/jephh-2-4-1.

Wang, L., Zhou, Y., Sun, X., Wu, S., Xia, L., Sun, J., Zha, Y., Yang, P., 2024. Retrieval of chromium and mercury concentrations in agricultural soils: using spectral information, environmental covariates, or a fusion of both? Ecol. Indic. 167, 112594. https://doi.org/10.1016/J.ECOLIND.2024.112594.

Wei, T., Simko, V., 2010. corrplot: visualization of a correlation matrix. In: *CRAN*: Contributed Packages. https://doi.org/10.32614/CRAN.package.corrplot.

Wickham, H., Averick, M., Bryan, J., Chang, W., McGowan, L., François, R., Grolemund, G., Hayes, A., Henry, L., Hester, J., Kuhn, M., Pedersen, T., Miller, E., Bache, S., Müller, K., Ooms, J., Robinson, D., Seidel, D., Spinu, V., Yutani, H., 2019. Welcome to the Tidyverse. J. Open Source Softw. 4 (43), 1686. https://doi.org/10.21105/joss.01686.

Xu, X., Wang, Z., Song, X., Zhan, W., Yang, S., 2024. A remote sensing-based strategy for mapping potentially toxic elements of soils: temporal-spatial-spectral covariates combined with random forest. Environ. Res. 240. https://doi.org/10.1016/j.envres.2023.117570.

Yang, G., Wang, L., Gu, W., Gu, J., Fan, D., Liang, M., Liu, J., Wang, Z., 2024. Soil ecological risk assessment of ten industrial areas in China based on the TRIAD and VIKOR methods. Ecol. Indic. 166, 112270. https://doi.org/10.1016/J.ECOLIND.2024.112270.

Yang, Y., Jia, M., 2024. 3D spatial interpolation of soil heavy metals by combining kriging with depth function trend model. J. Hazard. Mater. 461, 132571. https://doi.org/10.1016/J.JHAZMAT.2023.132571.

Zhang, Han, Cui, J., Xiong, Y., Li, G., Du, C., Zhang, L., 2025. Microbial response and the crucial function of predominant phyla in *Sedum alfredii*-mediated remediation of high concentration of multiple heavy metal soils. Environ. Pollut., 126211 https://doi.org/10.1016/J.ENVPOL.2025.126211.

Zhang, Hongxing, Mao, Z., Huang, K., Wang, X., Cheng, L., Zeng, L., Zhou, Y., Jing, T., 2019. Multiple exposure pathways and health risk assessment of heavy metal(loid)s for children living in fourth-tier cities in Hubei Province. Environ. Int. 129, 517–524. https://doi.org/10.1016/j.envint.2019.04.031.

Zhuang, P., Lu, H., Li, Z., Zou, B., McBride, M.B., 2014. Multiple exposure and effects assessment of heavy metals in the population near mining area in South China. PLoS One 9 (4). https://doi.org/10.1371/journal.pone.0094484.